Engineering Structures 264 (2022) 114408

Contents lists available at ScienceDirect

Engineering Structures

journal homepage: www.elsevier.com/locate/engstruct

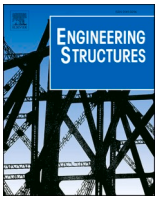

Shear enhancement in RC beams with stirrups simultaneously loaded within 2d and at 3d from supports

Marcus Vinicius Filiagi Pastore, Robert Lars Vollum *

Department of Civil and Environmental Engineering, Imperial College London, London, UK

ARTICLE INFO

Keywords:
Shear enhancement
Multiple point loads
Strut and tie
Design standards

ABSTRACT

Shear enhancement occurs in reinforced concrete (RC) beams when loads are applied within around 2*d* of supports where *d* is the beam effective depth. This paper examines shear enhancement in RC beams, with stirrups, which are loaded both within 2*d* of supports and at 3*d* from supports where shear enhancement is minimal. Simultaneously loading beams both inside and outside 2*d* of supports commonly occurs in practice but has not previously been systematically studied. A total of eight beams were tested in two groups of four having different reinforcement arrangements. The tests suggest that the shear resistance depends on the angle of the failure plane which is related to the loading arrangement. A strut and tie model (STM) is developed for analysing beams simultaneously loaded within and outside 2*d* of supports. The accuracy of the STM predictions is shown to be improved by relating strut strength to the strain in the flexural reinforcement. The proposed STM and nonlinear finite element analysis (NLFEA) with 3D solid elements are used to investigate parametrically the influence of loading arrangement on shear resistance. The strength predictions of the STM are shown to compare well with those of NLFEA. Comparisons are also made with shear strengths calculated using fib Model Code 2010 (MC2010) and the draft new generation of Eurocode 2 (prEN1992-1:21). The differing philosophies of these two methods are discussed.

1. Introduction

Considerable effort has been expended studying shear enhancement, due to arching action, in reinforced concrete deep beams loaded on their top face with point loads positioned within 2*d* of supports [1–9]. This research has led to the development of strut and tie models [2–7], nonlinear finite element models [7–8], kinematic [9] and mechanically based models [10–11] for shear resistance. Most tests on short shear span and deep beams have been carried out using three- or four-point loading with all loads applied within 2*d* of supports. Tests studying the influence of loading arrangement on shear resistance are scarce. Brown and Bayrak [6] tested a series of tests of deep beams of span 4.4*d* (3048 mm), without and with shear reinforcement, in which three statically equivalent asymmetrical loading arrangements were considered. The loading arrangements consisted of i) a single point load at 1.1*d* from the support, ii) two point loads at 0.55*d* and 1.67*d* and iii) a uniformly distributed load (udl) of length 2.2*d* with centroid at 1.1*d* from the support. The tests showed that the failure load was greatest for the udl as found for slender beams in [12]. Brown and Bayrak [6] concluded that that "different load-carrying mechanisms are present for different load distributions" but the udl could be represented by two point loads. Tests on beams loaded with pairs of point loads applied within 2*d* of supports have also been undertaken by Vollum and Fang [3] as well as Elwakeel and Vollum [4] who likewise found the load carrying mechanism to depend on the loading arrangement. In practice, slender beams can be loaded with concentrated loads applied both within and outside 2*d* of supports as shown in Fig. 1 for a cross-head girder. This type of loading also arises in transfer beams supporting planted columns but is scarcely researched. Way back in 1956, Ferguson [13] carried out an exploratory campaign to investigate the influence of loading arrangement on shear enhancement in beams without shear reinforcement. Despite this, the authors are only aware of one previous test campaign that considered the shear strength of slender beams, with shear reinforcement, loaded both within and outside 2*d* of supports. Bryant et al. [14] tested pairs of two span continuous beams with shear reinforcement and either three or five loads in each shear span. All these beams failed in flexure so do not give insight into shear resistance.

The present research was motivated by differences between the

* Corresponding author.
E-mail address: r.vollum@imperial.ac.uk (R.L. Vollum).

https://doi.org/10.1016/j.engstruct.2022.114408
Received 13 December 2021; Received in revised form 30 March 2022; Accepted 12 May 2022
Available online 28 May 2022

design approaches adopted for shear enhancement in EC2 [15] and previous UK practice [16] which become particularly pertinent for load cases like that shown in Fig. 1. EC2 [15] and fib Model Code 2010 (MC2010) [17] reduce the contribution to the design shear force of concentrated loads applied to the top of a beam within 2*d* of supports by a multiple $\beta = a_v/2d$ where a_v is the clear shear span. Conversely, the superseded UK code BS8110 [16], as well as the draft next generation EC2 (prEN1992-1:21) [18], relate the shear resistance within 2*d* of the support to the angle of the failure plane which is assumed to have a horizontal projection of a_v. Enhancing the shear resistance near to supports is attractive from a design perspective because it decouples the calculation of design shear force and shear resistance. The paper examines the realism of these differing approaches to modelling shear enhancement through an experimental campaign, nonlinear finite element modelling and strut and tie modelling.

2. Experimental program

Eight beams were tested with shear reinforcement. The loading arrangement was chosen to simulate the case of a beam that is simultaneously loaded near the support and elsewhere within the span. The point load at 3*d* in the test set up is intended to represent the resultant effect of loads applied outside 2*d* of supports. The beam depth of 500 mm was chosen to be the same depth as adopted in previous investigations into shear enhancement by Vollum [2–4]. The loading ratios were chosen to investigate the interaction between loads applied within and outside 2*d* of supports. The beams spanned 3350 mm between support centrelines and measured 500 mm deep × 250 mm wide. The beams with shear reinforcement were divided into two series of four with series 1 having flexural tension reinforcement consisting of 4B25 bars in a single layer (Fig. 2a) and series 2 having two layers of 3B25 bars (Fig. 2b). The top longitudinal reinforcement in both series consisted of two B16 straight bars. Beams in series 1 had B8 stirrups at 200 mm centres while beams in series 2 had B8 stirrups at 300 mm centres.

The loading arrangements (see Table 1) were chosen to systematically investigate the influence of varying the ratio of the loads applied within and outside 2*d* of supports. In each series of tests, a pair of control beams were tested with single point loads at either 1.5*d* or 3*d* from the left hand support. All but one of the remaining tests investigated the influence of loading the beams with pairs of concentrated loads applied in various ratios at 1.5*d* and at 3*d* from the left support (Fig. 2a, b). In the remaining test, the beam was loaded with equal point loads applied at 1.1*d* and 1.9*d* (Fig. 2c) giving a resultant force at 1.5*d*. Steel loading and support plates were adopted with dimensions of 250 wide × 100 long × 30 thick mm^3. The naming convention of the specimens describes the beam loading arrangement and reinforcement as follows:

2P - two point loads (P_1 and P_2).
1.5d/3d – P_1 applied at 1.5*d* and P_2 at 3*d* from the centre of the support.
20:80 – 20% of the total load applied at P_1 and the remaining 80% at P_2.
2x3ϕ25 – Bottom longitudinal reinforcement composed of two layers of three 25-mm bars.
s3 –stirrups at 300 mm centres.

2.1. Material properties

The beams were cast in two groups of four from ready mixed concrete with specified strength class C25/30. There was an unintended switch between the coarse aggregate types used in series 1 and 2 with 20 mm limestone aggregate used in series 1 and 20 mm gravel aggregate in series 2. This is not considered to have significantly affected the results since the coarse aggregate was the same size in series 1 and 2 and did not fracture. Control specimens for each series of four beams consisted of 12 cylinders (100 mm × 200 mm) and 12 cubes (100 mm) for compressive strength tests and 12 cylinders (150 mm × 300 mm) for tensile splitting strength. After casting, half of each type of specimen were cured in air alongside the beams with the remainder cured in water at 20 °C. The air cured specimens were covered with polythene sheets and sprayed with water every other day for two weeks. Half of the cylinders were tested at

Fig. 1. "Mirassolandia" precast concrete bridge in Sao Jose do Rio Preto, SP, Brazil (reproduced with permission of www.migliorepastore.com.br.).

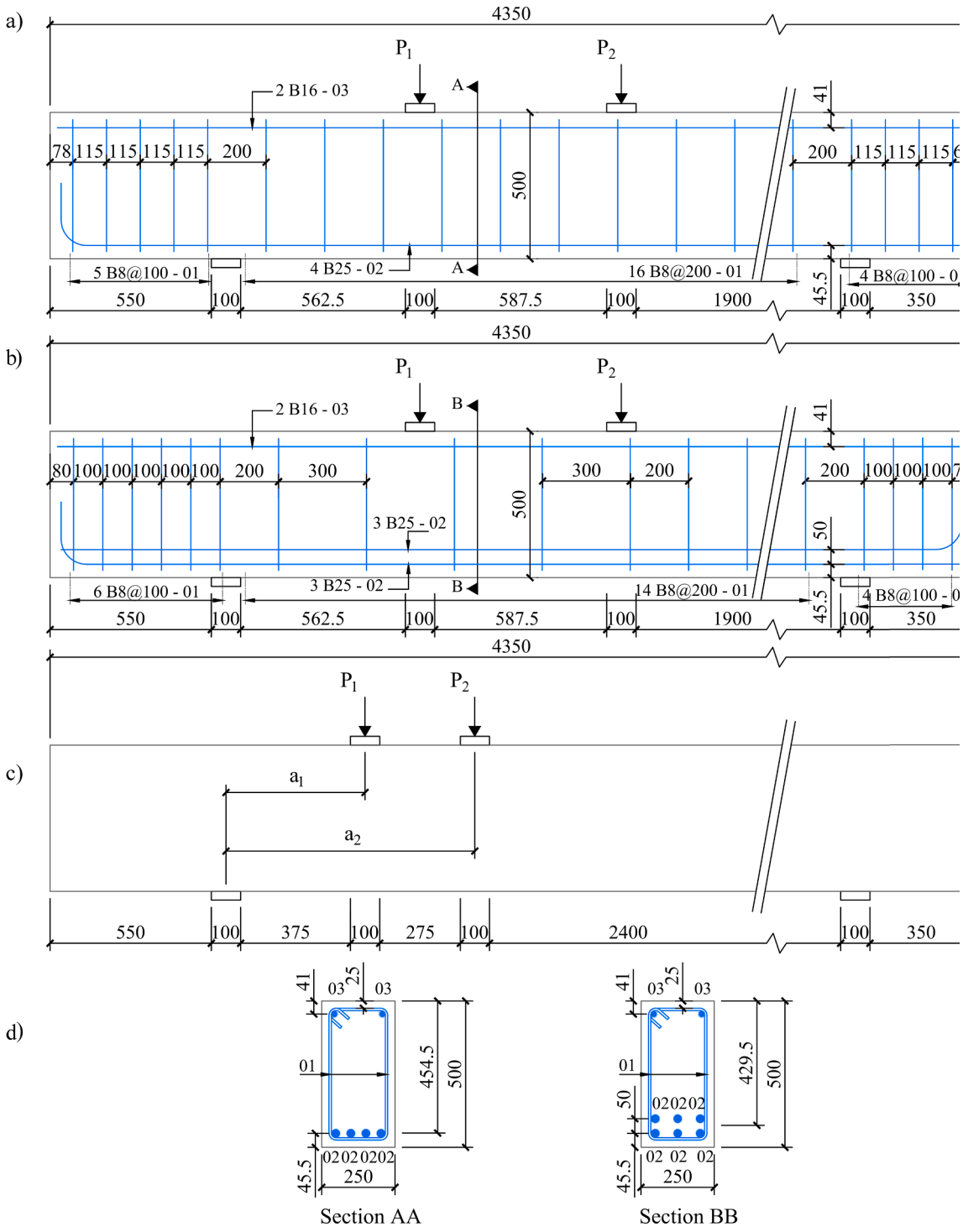

Fig. 2. Geometry and typical loading arrangements of the beams: a) Beams with 8-mm stirrups at 200 mm centres, b) Beams with 8-mm stirrups at 300 mm centres, c) loading arrangement for 2P-1.1d/1.9d-50:50-4ϕ25s2 and d) cross-section details.

the same time as the first beam of each series with the remainder tested at the same time as the last beam of each series. The measured concrete strengths at the time of testing the first and last beam of each series are summarised in Table 2. It is unknown why the air cured cylinder strengths are slightly higher than the water cured strengths but the difference is not considered significant. Table 3 lists the measured tensile properties of the reinforcement which were determined in accordance with [19].

2.2. Beam setup and test procedure

The beams were loaded in an internal reaction frame through a single 1000-kN hydraulic jack operating in displacement control. Pairs of loads were applied through a spreader beam as shown in Fig. 3. The ratio between the loads applied at 1.5*d* and 3*d* was varied by moving the beam leftward or rightward within the loading rig which was fixed in position. The beams were supported on bearings which allow both rotation and horizontal movement. Load was applied at a rate of around 0.2 mm/minute which on average corresponded to a loading rate of

Table 1
Description of the beams.

Beam	Effective depth (mm)	A_s [a]	Stirrups	Loading arrangement
P-1.5d-4ϕ25s2	454.5	4B25	B8 at 200 mm	Fig. 1a - P_1 = 100%, P_2 = 0%
2P-1.1d/1.9d-50:50-4ϕ25s2	454.5	4B25	B8 at 200 mm	Fig. 1c - P_1 = 50%, P_2 = 50%
2P-1.5d/3d-40:60-4ϕ25s2	454.5	4B25	B8 at 200 mm	Fig. 1a - P_1 = 40%, P_2 = 60%
P-3d-4ϕ25s2	454.5	4B25	B8 at 200 mm	Fig. 1a - P_1 = 0%, P_2 = 100%
2P-1.5d/3d-60:40-4ϕ25s2[b]	454.5	4B25	B8 at 200 mm	Fig. 1a - P_1 = 60%, P_2 = 40%
P-1.5d-2x3ϕ25s3	429.5	6B25 in 2 layers	B8 at 300 mm	Fig. 1b - P_1= 100%, P_2 = 0%
P-3d-2x3ϕ25s3	429.5	6B25 in 2 layers	B8 at 300 mm	Fig. 1b - P_1 = 0%, P_2 = 100%
2P-1.5d/3d-40:60-2x3ϕ25s3	429.5	6B25 in 2 layers	B8 at 300 mm	Fig. 1b - P_1 = 40%, P_2 = 60%
2P-1.5d/3d-20:80-2x3ϕ25s3	429.5	6B25 in 2 layers	B8 at 300 mm	Fig. 1b - P_1 = 20%, P_2 = 80%

[a] Flexural tension reinforcement, [b] re-test of 2P-1.5d/3d-40:60-4ϕ25s2.

Table 2
Mean concrete strengths.

Series	test order	Compressive cylinder strength		Tensile strength	
		$f_{c,avg,water}$ (MPa)	$f_{c,avg,air}$ (MPa)	$f_{t,avg,water}$ (MPa)	$f_{t,avg,air}$ (MPa)
1	first	27.7	29.3	2.3	2.0
	last	30.1	32.0	2.5	2.1
2	first	29.7	31.0	2.3	2.1
	last	30.3	32.0	2.5	2.1

Table 3
Steel reinforcement properties.

Diameter (mm)	E_s (MPa)	f_y (MPa)	ε_{yield}* (mm/m)	f_u (MPa)	ε_{su}^{**} (mm/m)
8	200,100	510	2.5	695	136
16	194,900	550	2.8	645	147
25	200,600	540	2.7	650	126

* Reinforcement yielding, ** Reinforcement fracture strain.

around 12 kN/minute. Following flexural yielding in beam 2P-1.5d/3d-40:60-4ϕ25s2, and post failure in the other beams, the loading rate was increased to around 0.4 mm/minute since the peak load had been reached. Load cells (LC) were positioned under each loading point and under the left hand support to determine the reaction. Other instrumentation included strain gauges attached to the stirrups and longitudinal bars and linear variable displacement transducers (LVDT) measuring displacements and beam end rotations.

In this paper, Digital Image Correlation (DIC) is used to illustrate the development of cracking. Although not reported here, DIC was used to record displacement fields from which crack opening and sliding displacements were calculated. The crack opening and sliding displacements were subsequently used to determine the components of shear force resisted within the critical shear crack by residual concrete tensile strength, aggregate interlock, dowel action, stirrups and the flexural compressive zone [20].

3. Test results and discussion

3.1. Series 1: Beams with 8-mm stirrups at 200 mm centres

The loading arrangements for series 1 are summarised in Table 4 along with the concrete strengths at the time of testing and failure loads. A total of five tests were carried out on the four beams of series 1 since beam 2P-1.5d/3d-40:60-4ϕ25s2 was repaired and retested as 2P-1.5d/3d-60:40-4ϕ25s2 after initially failing in flexure. All the beams failed in shear except for 2P-1.5d/3d-40:60-4ϕ25s2 and 2P-1.5d/3d-60:40-4ϕ25s2 which failed in flexure. The concrete compressive strengths given in Table 4 are averages of the air and water cured cylinder strengths. The concrete strengths of the second and third tested beams were found by linear interpolation between the strengths of the first and last tested beams.

Fig. 4 shows the principal tensile strains obtained with DIC using [21] at i) peak load and ii) after failure when the final crack pattern had formed. The maximum principal strain occurs normal to the cracks so the strain magnitude over the selected subset size of 31 pixels is an indication of crack width. Fig. 5 shows photographs of the beams after failure. Significantly, the shear resistance of beam 2P-1.1d/1.9d-50:50-4ϕ25s2 was 633 kN compared with 387 kN for beam P-1.5d-4ϕ25s2 which had statically equivalent loading. This shows that it can be very conservative to replace multiple point loads positioned within 2*d* of the support by their resultant when assessing shear resistance. In both beams, the major shear crack at failure ran from the outside edge of the support to the inside edge of the adjacent loading plate at P_1. The failure mode of both beams was characteristic of shear-compression but the crack development was different. In beam 2P-1.1d/1.9d-50:50-4ϕ25s2, the critical diagonal shear crack (depicted "1" in Fig. 4a) formed at V = 170 kN ($0.27V_{max}$). Near maximum load, crack "2" in Fig. 4a rapidly extended to the loading plate at P_1 causing complete failure. In beam, P-1.5d-4ϕ25s2 the critical shear crack formed at V = 150 kN ($0.39V_{max}$). This crack ("1") subsequently merged with the upper diagonal crack ("2") shown in Fig. 4c causing complete failure. The significantly greater shear strength of 2P-1.1d/1.9d-50:50-4ϕ25s2 compared with P-1.5d-4ϕ25s2 results from the steeper orientation of the failure crack in 2P-1.1d/1.9d-50:50-4ϕ25s2 (see Fig. 5a and b).

In beam 2P-1.5d/3d-40:60-4ϕ25s2, the dominant shear crack ("1" in Fig. 4e and Fig. 5c) developed from the flexural shear crack closest to the support at $0.30V_{max}$ = 150 kN and subsequently extended outwards towards the nearest edges of the support and inner loading plate. Both the bottom and top reinforcement yielded near to the maximum load. Subsequently, a shallow "V" shaped crack ("2" in Fig. 4f) developed under the loading plate at P_2. This was followed by crushing of the concrete in the flexural compression zone. The beam was repaired with a high strength grout and re-tested as beam 2P-1.5d/3d-60:40-4ϕ25s2 with the loads in the same position but with loading ratio changed to 60:40. Beam 2P-1.5d/3d-60:40-4ϕ25s2 also failed in flexure (Fig. 4g,h). Consequently, the measured shear strength of these beams is a lower bound. The localised change in the material properties due to the repair was not modelled in the structural analysis of the beams presented in this paper.

Beam P-3d-4ϕ25s2 with a single load at 3*d* failed in shear with the least resistance of 297 kN. The critical shear crack ("1" in Fig. 4i) developed from a flexural shear crack at V = 114 kN ($0.38V_{max}$). Subsequently, this crack extended upwards towards the corner of the loading plate and horizontally along the flexural reinforcement towards the support until it merged with a small flexural crack ("2" in Fig. 4i) at peak load.

3.2. Series 2: Beams with 8-mm stirrups at 300 mm centres

To avoid flexural failure, the stirrup spacing in series 2 was increased to 300 mm and the bottom reinforcement was increased to six 25 mm diameter bars provided in two layers. Similarly to series 1, beam P-1.5d-

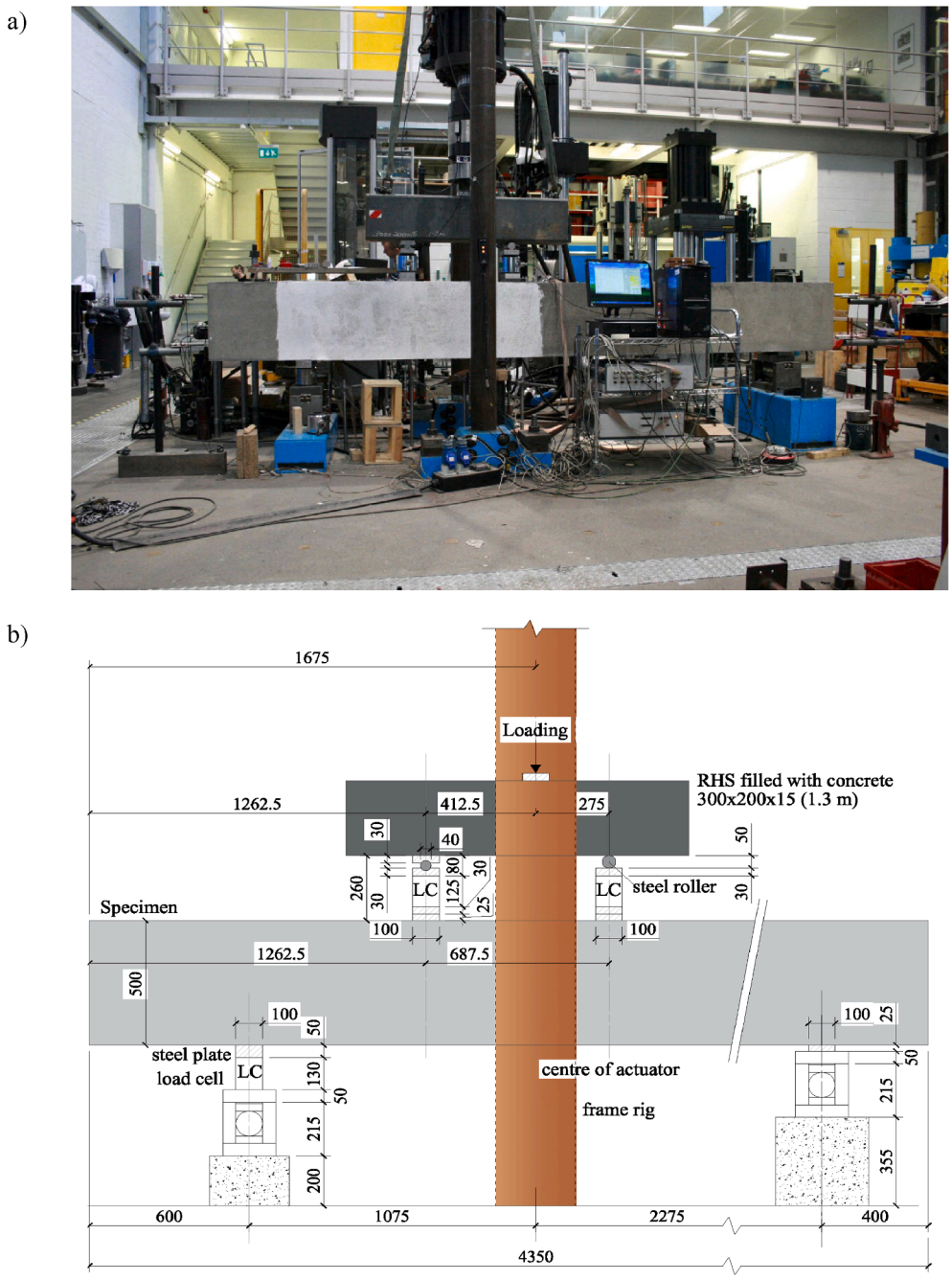

Fig. 3. Test rig setup for beam 2P-1.5d/3d-40:60-4ϕ25s2.

Table 4
Summary of experimental results of beams with 8-mm stirrups at 200 mm centres.

Beam	Age at test	f_c [a]	f_t [b]	Aggregate		d	V_{test} [c]	V_{flex} [d]	Failure
	(days)	(MPa)		type	(mm)	(mm)	kN	kN	Mode
P-1.5d-4ϕ25s2	28	28.5	2.2	limestone	20	454.5	387	639	Shear
2P-1.1d/1.9d-50:50-4ϕ25s2	31	28.9	2.2	limestone	20	454.5	633	688	Shear
2P-1.5d/3d-40:60-4ϕ25s2	32	29.0	2.2	limestone	20	454.5	492	449	Flexure
P-3d-4ϕ25s2	36	29.0	2.2	limestone	20	454.5	297	314	Shear
2P-1.5d/3d-60:40-4ϕ25s2[e]	51	31.1	2.3	limestone	20	454.5	531	550	Flexure

[a] Compressive strength of concrete used in calculations.
[b] Tensile strength of concrete used in calculations.
[c] Neglecting shear force due to self-weight of 5 kN.
[d] Calculated with M_r = 423 kNm.
[e] Re-test of 2P-1.5d/3d-40:60-4ϕ25s2.

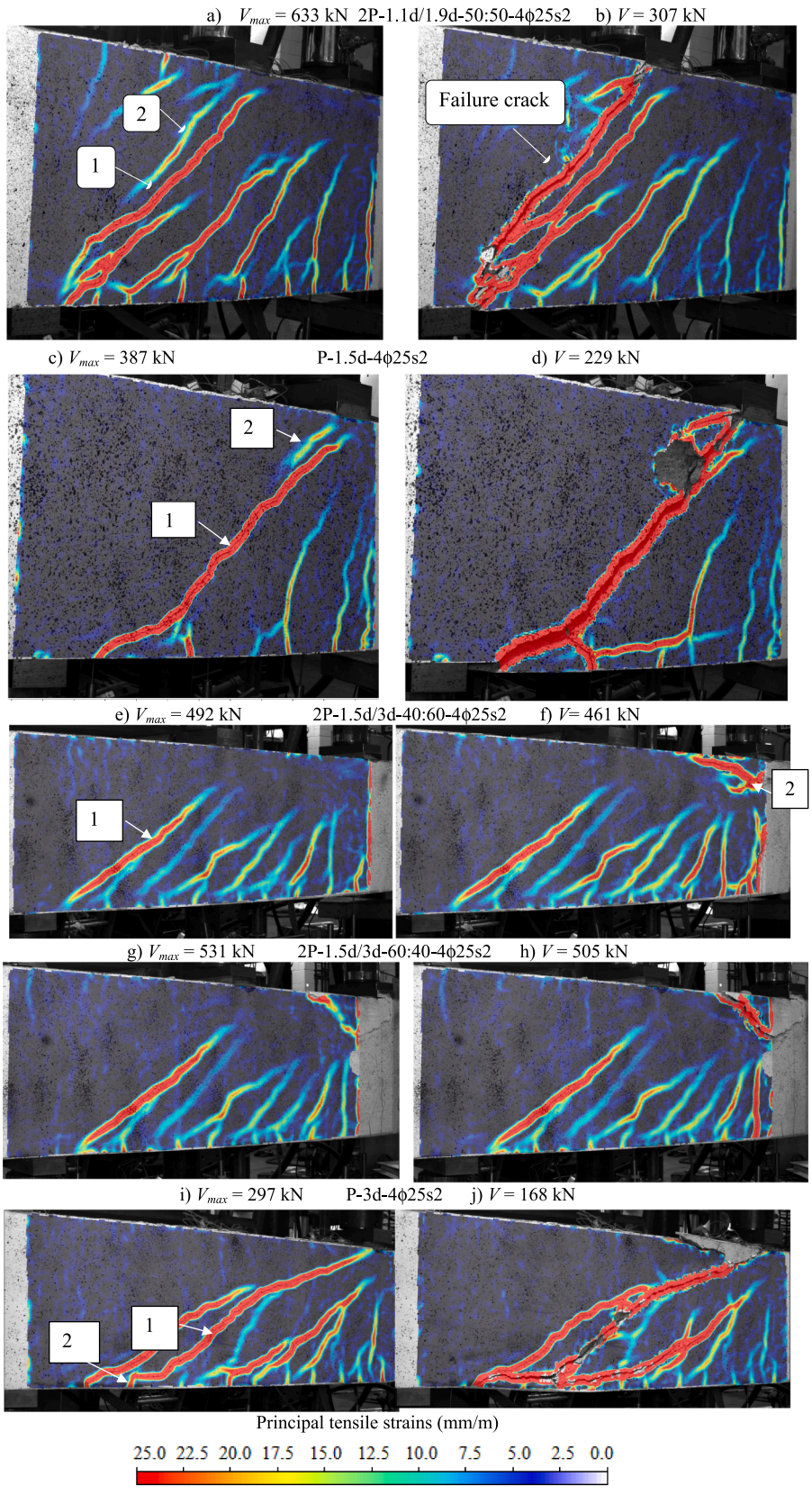

Fig. 4. Crack patterns and strain state at peak load and after failure for beams with 8-mm stirrups at 200 mm centres.

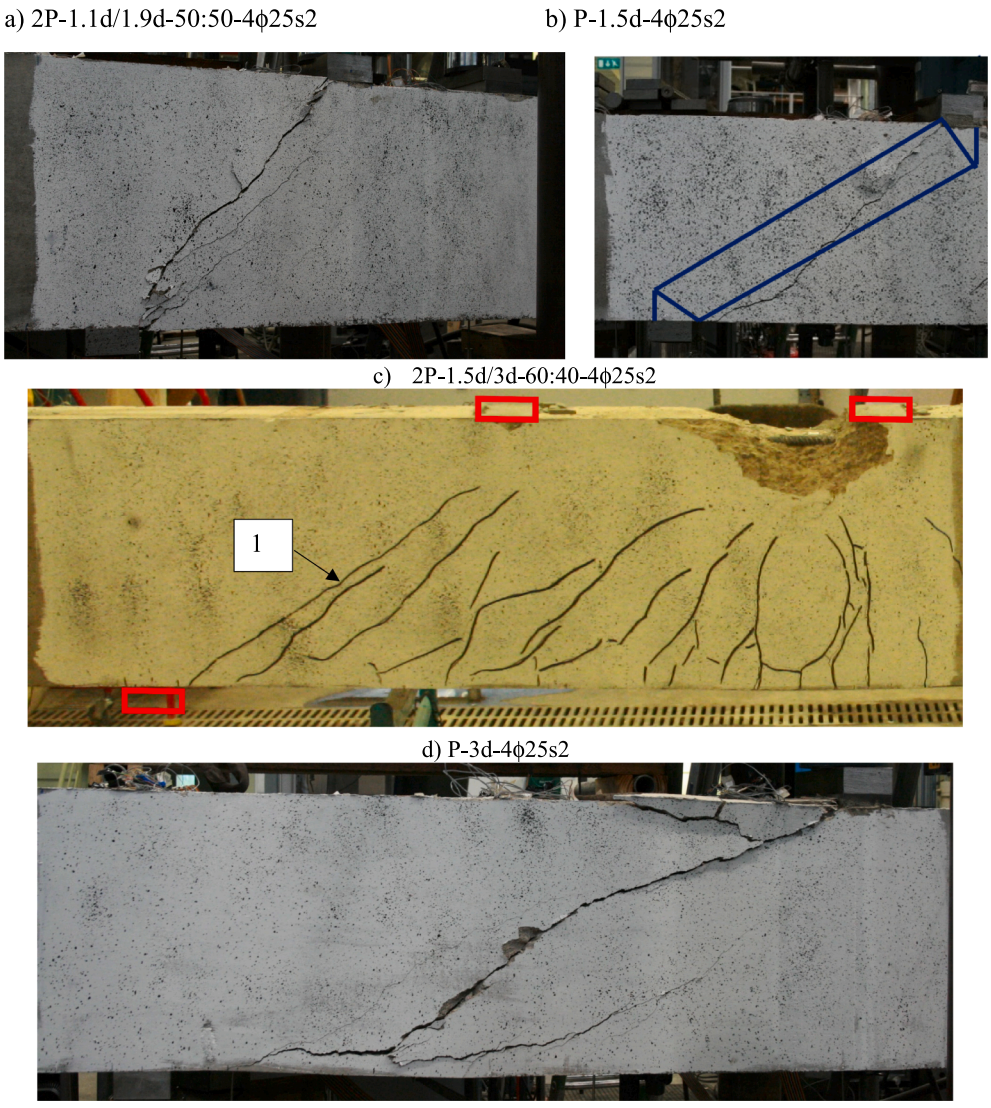

Fig. 5. Final crack patterns for beams of Series 1 with 8-mm stirrups at 200 mm centres.

2x3ϕ25s3 was loaded at 1.5*d* and beam P-3d-2x3ϕ25s3 at 3*d*. The remaining two beams were simultaneously loaded at 1.5*d* and 3*d* with loading proportions of 1:1.5 (2P-1.5d/3d-40:60-2x3ϕ25s3) and 1:4 (2P-1.5d/3d-20:80-2x3ϕ25s3). All the beams failed in shear at the maximum shear forces given in Table 5 which also gives concrete strengths.

The principal tensile strains at i) peak load and ii) post failure are shown for series 2 in Fig. 6 while Fig. 7 shows the final crack pattern for each test. The failure modes of beams P-1.5d-2x3ϕ25s3 and 2P-1.5d/3d-40:60-2x3ϕ25s3 were characteristic of shear-compression but the crack development differed. The critical shear crack in beam P-1.5d-2x3ϕ25s3 ("1" in Fig. 6a) formed at $V = 180$ kN ($0.36V_{max}$). Subsequently, the crack extended steadily outwards towards the nearest corners of loading and bearing plates (Fig. 6a). A secondary shear crack "2" developed at the inner corner of the loading plate near maximum load. There was no unique single failure crack as evident in Fig. 6b. Notably, beam P-1.5d-2x3ϕ25s3 (Fig. 6a,b) failed at $V = 496$ kN which is significantly greater than its companion P-1.5d-4ϕ25s2 from series 1 which failed at $V = 387$ kN despite having similar concrete strength and closer stirrup spacing. This appears to be due to the different shape of the critical shear crack in both beams. In Fig. 5b, the critical shear crack cuts the theoretical direct

Table 5
Summary of experimental results of beams with 8-mm stirrups at 300 mm centres.

Beam	Age at test	f_c [a]	f_t [b]	Aggregate		d	V_{test} [c]	V_{flex} [d]	Failure
	(days)	(MPa)		type	(mm)	(mm)	kN	kN	Mode
P-1.5d-2x3ϕ25s3	46	30.8	2.2	sea dredged gravel	20	429.5	496	833	Shear
P-3d-2x3ϕ25s3	49	30.9	2.3	sea dredged gravel	20	429.5	287	409	Shear
2P-1.5d/3d-40:60-2x3ϕ25s3	50	31.0	2.3	sea dredged gravel	20	429.5	510	585	Shear
2P-1.5d/3d-20:80-2x3ϕ25s3	56	31.1	2.3	sea dredged gravel	20	429.5	387	487	Shear

[a] Compressive strength of concrete used in calculations.
[b] Tensile strength of concrete used in calculations.
[c] Neglecting shear force due to self-weight of 5 kN.
[d] Calculated with moment of resistance $M_r = 552$ kNm.

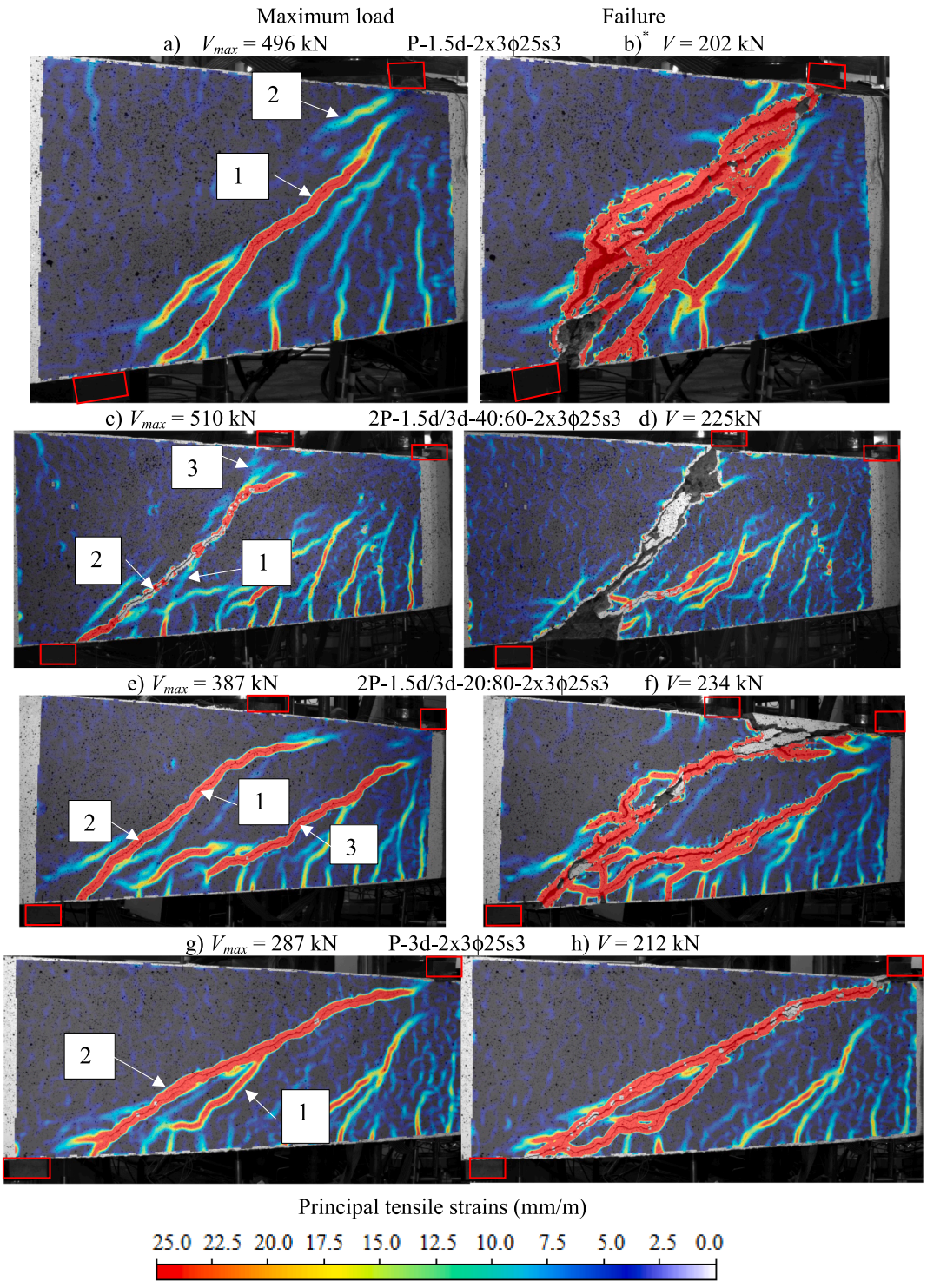

Fig. 6. Crack patterns and strain state at peak load and after collapse for series 2 with 8-mm stirrups at 300 mm centres.

strut, while in Fig. 7a it runs parallel to the direct strut allowing more load to go directly to the support. This suggests that shear enhancement due to arching action is sensitive to random variations in the position and orientation of the critical shear crack to the direct strut as found by others [2,22].

The critical shear crack in 2P-1.5d/3d-40:60-2x3ϕ25s3 developed from the merging of cracks "1" and "2" in Fig. 6c. Crack "1" is a flexural shear crack which initiated at $V = 180$ kN ($0.35V_{max}$) while crack "2" is a shear crack. The failure crack (Fig. 6d) resulted from the merging of the critical shear crack and the secondary shear crack adjacent to the inner corner of the loading plate ("3") which formed just before the peak load (Fig. 6c).

The critical shear crack in 2P-1.5d/3d-20:80-2x3ϕ25s3 (Fig. 6e,f) developed from the merging of a flexural shear crack ("1") and a shear crack ("2") at $V = 170$ kN ($0.44V_{max}$). The flexural shear crack initiated in the soffit of the beam at a distance of 215 mm from the support at $V =$ 135 kN ($0.35V_{max}$). The shear crack initiated at the inner corner of the bearing plate at $V = 150$ kN ($0.39V_{max}$). From $V = 250$ kN ($0.65V_{max}$),

a) P-1.5d-2x3ϕ25s3

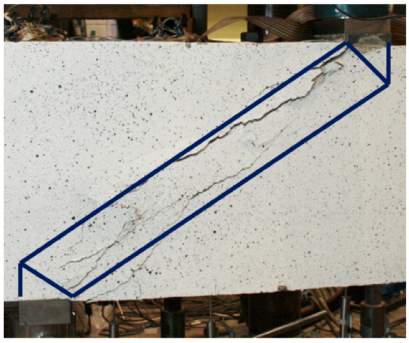

b) 2P-1.5d/3d-40:60-2x3ϕ25s3

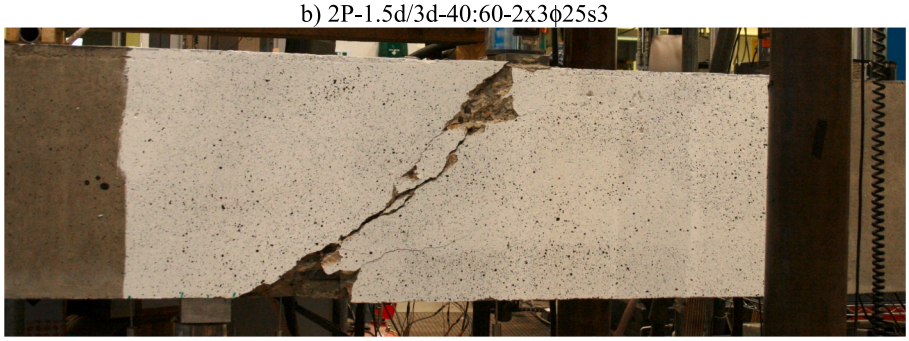

c) 2P-1.5d/3d-20:80-2x3ϕ25s3

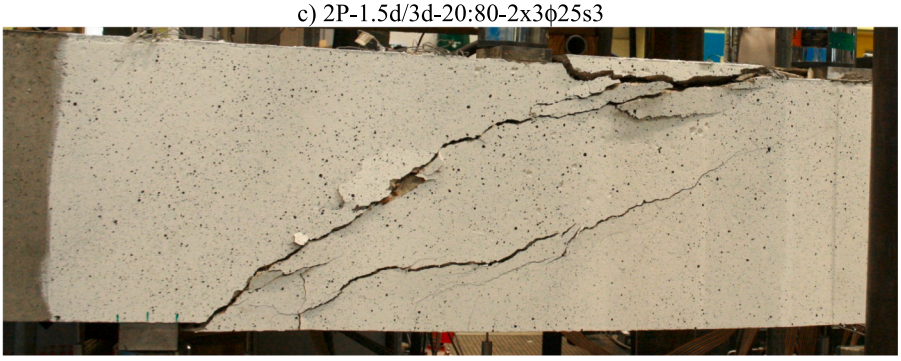

d) P-3d-2x3ϕ25s3

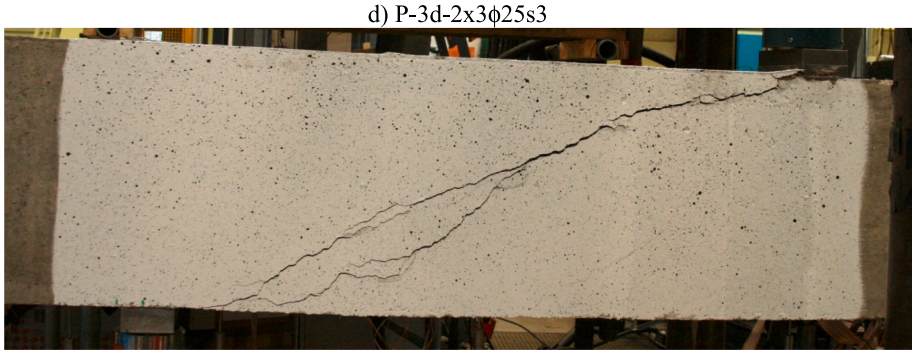

Fig. 7. Final crack patterns for each beam with 8-mm stirrups at 300 mm centres.

three of the flexural shear cracks between the two point loads widened and extended eventually coalescing to form crack "3" which became the second widest shear crack. At maximum load, the critical shear crack extended rapidly towards the inner edge of the outer loading plate causing the final crack pattern (Fig. 6f). The maximum shear force was 387 kN, which lies between that for beams P-1.5d-2x3ϕ25s3 (500 kN) and P-3d-2x3ϕ25s3 (287 kN).

Beam P-3d-2x3ϕ25s3 (Fig. 6g,h), with a single point load at 3*d*, failed at the lowest shear force as expected. Similarly to beam 2P-1.5d/3d-20:80-2x3ϕ25s3, the critical shear crack developed from the merging of a flexural shear crack ("1" in Fig. 6g) and a shear crack ("2" in Fig. 6g) adjacent to the support. Crack 1 first formed in the beam soffit 425 mm from the inner corner of the bearing plate at 130 kN ($0.45V_{max}$). Crack 2 formed at $V = 160$ kN ($0.56V_{max}$) and shortly afterwards merged with crack 1 to form the critical shear crack. At maximum load, the tip of the critical shear crack was only around 10 mm short of the loading plate (Fig. 6g).

4. Strut and tie modelling

Refined STM, depicted STMa and STMb in Fig. 8, were developed by the authors for the tested beams and are applicable respectively to cases where the stirrups in the inner shear span i) cannot and ii) can solely resist the shear force V in the outer shear span (i.e. between P_1 and P_2 in Fig. 2). In STMa, the load P is transferred directly to the support through strut I. The shear force V in the outer shear span is transferred into struts II and III through ties T_{s2} and T_{s1} respectively. STMb, which differs from that of Sagaseta and Vollum [2] in the inclusion of the shear force V at the right hand side of the free body diagram, is applicable if $T_{s1} \geq V$ (where T_{s1} denotes the yield capacity of the stirrups in the inner shear span a_{v1}). In this case, part of the load P is resisted by Strut II which is indirect. STMa and STMb converge when $T_{s1} = V$ in which case strut II disappears in both STMs.

The failure load is the least corresponding to flexure, shear and bearing failure under the loading and support plates. The stress at the back of the bottom node is not considered critical as implied by Figure 6.27 of EC2 [15] and Figure 7.3–39 of MC2010 [17]. Concrete controlled shear failure in STMa arises due to either crushing of Strut I at its top end or by crushing of Strut II at its bottom end. Strut III is not critical since it is steeper than strut I. Concrete controlled shear failure in STMb occurs due to crushing of Strut I at the critically stressed end which in general depends on the bearing plate widths. The node geometry and strut forces are shown in Fig. 9. Tables 6 to 8 give the design concrete design strengths at the top and bottom nodes respectively according to EC2 [15], the Modified Compression Field Theory (MCFT) [23] and prEN 1992-1-1: 2021 [18,24]. The symbols in Tables 6 and 7 are defined in Table 8.

4.1. Derivation of design equations and solution for STMa

The maximum shear force is given by Eq. (1), where P is the point-load applied within 2d of supports and V is the shear force in the outer shear span between P_1 and P_2.

$$V_{max} = P + V = P{\cdot}(1+\kappa) \tag{1}$$

where κ is defined in terms of the loading arrangement as follows:

$$\kappa = \frac{V}{P} \tag{2}$$

The load P is limited by concrete crushing in strut I. Failure only needs to be considered at the top node of strut I since failure of strut II is critical at the bottom node. Failure of strut I at the top node, which is not critical for the tested beams, gives:

$$P \leq b{\cdot}f_{cst}{\cdot}w_{I,top}{\cdot}sin\beta_I \tag{3}$$

where b is the beam width, $w_{I,top}$ is the width of strut I, normal to its centreline at the top node, f_{cst} is the strength of Strut I at the top node and β_I is the inclination of Strut I to the horizontal.

Vertical equilibrium gives:

$$V = T_{s1} + T_{s2} = \frac{A_{sw}}{s_w}{\cdot}f_{yw}{\cdot}(a_{v1} + l_t + a_{v2}) = \frac{A_{sw}}{s_w}{\cdot}f_{yw}{\cdot}0.9d{\cdot}cot\theta \tag{4}$$

where T_{s1} is the resultant tensile force in the stirrups in the inner shear span (a_{v1}), T_{s2} is the resultant tensile force in the stirrups in the outer shear span (a_{v2}), A_{sw} is the cross-sectional area of each set of stirrups at spacing s_w and f_{yw} is the yield strength of the stirrups. The force T_{s2} is determined in the solution procedure and is limited by the compressive resistance of strut II at the bottom node. In the definition of model geometry, the dimensions e_{s1} and e_{s2} in Fig. 8a are defined as $e_{s1} = 0.5a_{v1}$

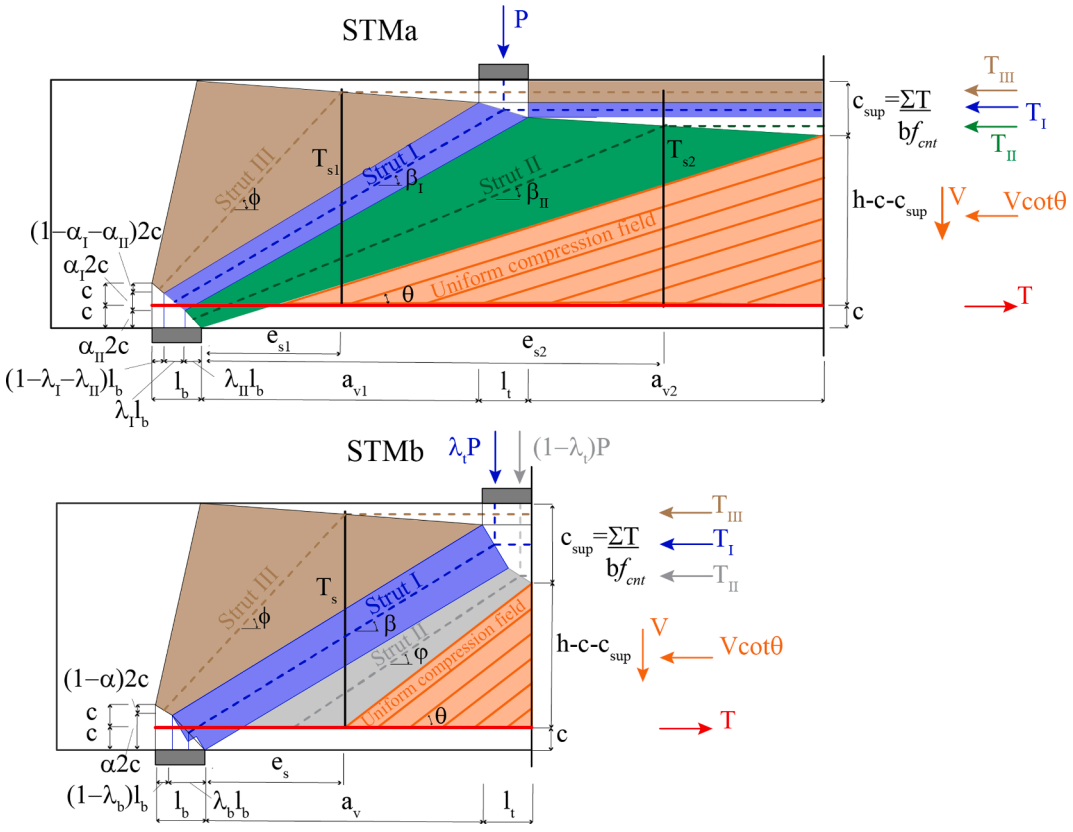

Fig. 8. Proposed STM for loading arrangement with shear force from point-load near supports (P) and from loads far from supports (V). STMa is valid for $T_{s1} \leq V$ and STMb is used otherwise.

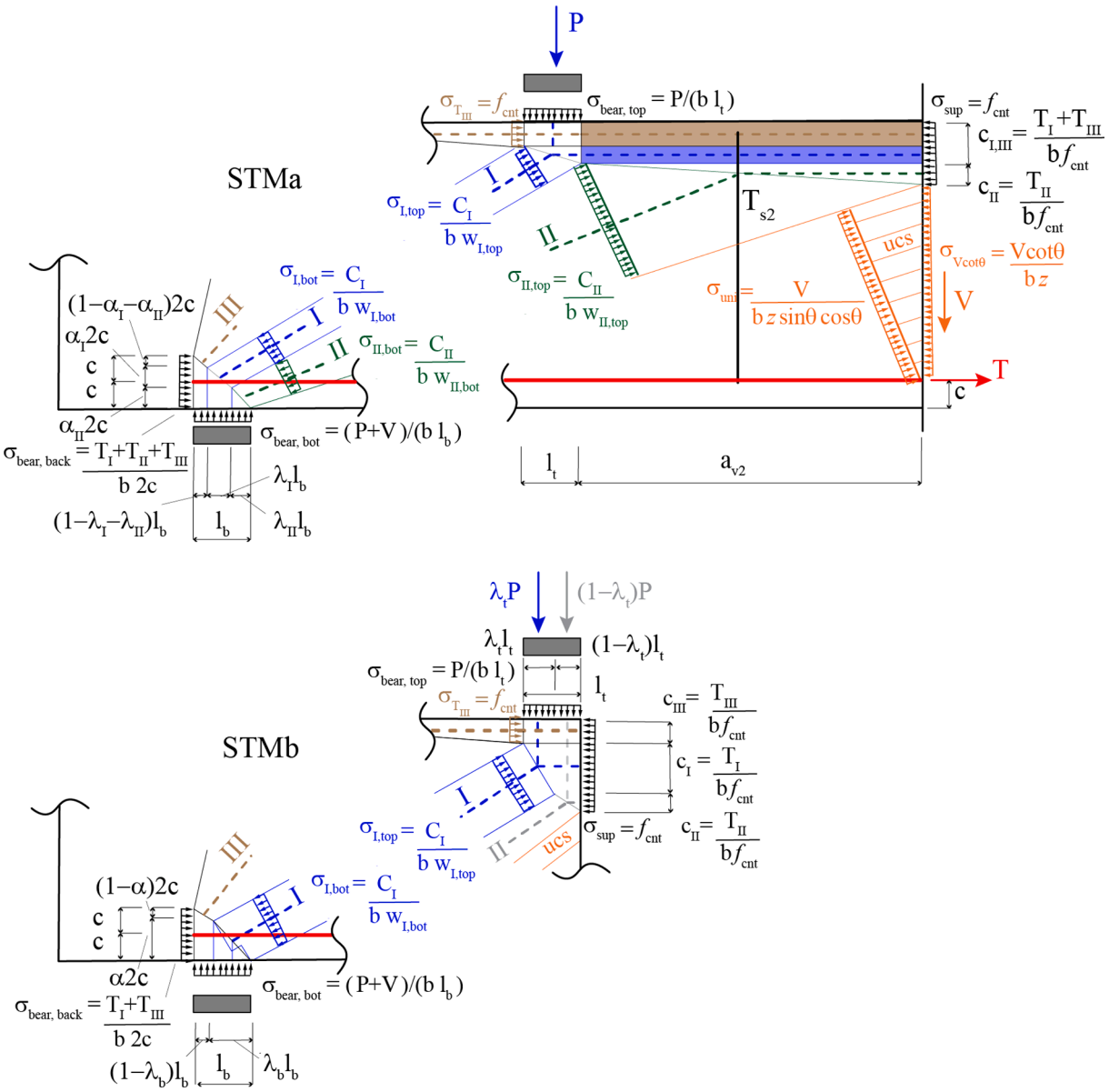

Fig. 9. Node geometry and strut forces at top and bottom nodes for STMa and STMb.

Table 6
Maximum allowable stress at the top node (CCC)[a].

	Strut *I*	Strut *II* STMb	Bearing under plate	Flexural compressive stress (f_{cnt})
Eurocode 2 [15]	νf_{cd}	νf_{cd}	νf_{cd}	νf_{cd}
MCFT [23]	$0.85 f_{cd}$	$0.85 f_{cd}$	$0.85 f_{cd}$	$0.85 f_{cd}$
prEN 1992-1-1: 2021 [18]	$\eta_{fc} f_{cd}$	$\eta_{fc} f_{cd}$	$\eta_{fc} f_{cd}$	$\eta_{fc} f_{cd}$

[a] $f_{cd} = f_{ck}/\gamma_c$ where γ_c is the partial factor for concrete which is taken as 1.0 in this paper.

Table 7
Maximum allowable stress at the bottom node (CCT)[a].

	Strut I cracked strut	Strut II cracked strut	Strut III uncracked strut	Bearing under plate
EC2 [15]	$0.6\nu f_{cd}$	$0.6\nu f_{cd}$	$0.85\nu f_{cd}$	$0.85\nu f_{cd}$
MCFT [23]	$k_c f_{cd}$	$k_c f_{cd}$	$0.85 f_{cd}$	$0.85 f_{cd}$
prEN 1992-1-1: 2021 [18]	$k_e \eta_{fc} f_{cd}$	$k_e \eta_{fc} f_{cd}$	$\eta_{fc} f_{cd}$	$\eta_{fc} f_{cd}$

[a] $f_{cd} = f_{ck}/\gamma_c$ where γ_c is the partial factor for concrete which is taken as 1.0 in this paper.

and $e_{s2} = a_{v1} + l_t + 0.5a_{v2}$.

The proportion of the bottom bearing plate length (l_b) supporting Strut I is given by:

$$\lambda_I = \frac{P}{P+V} = \frac{1}{1+\frac{V}{P}} = \frac{1}{1+\kappa} \tag{5}$$

The proportion of the bottom bearing plate length (l_b) supporting Strut II is given by:

$$\lambda_{II} = \frac{T_{s2}}{P+V} = \frac{\frac{A_{sw}}{s_w} f_{yw} \cdot a_{v2}}{P+V} = \frac{1 - \frac{a_{v1}+l_t}{0.9d \cdot cot\theta}}{1+1/\kappa} \tag{6}$$

where T_{s2} is the resultant tensile force of stirrups in the outer shear span, l_t is the length of the loading plate, a_{v1} is the clear inner shear span and:

$$a_{v2} = 0.9d \cdot cot\theta - (a_{v1} + l_t) \tag{7}$$

Table 8
Efficiency factors in Tables 6 and 7.

EC2 [15]	$\nu = 1 - \frac{f_{ck}}{250}$
MCFT [23]	$k_\varepsilon = \frac{1}{0.8 + 170\varepsilon_1}$ $\varepsilon_1 = \varepsilon_x + (\varepsilon_x + 0.002)cot^2\beta$
prEN 1992-1-1: 2021 [18]	$\eta_{fc} = \left(\frac{40}{f_{ck}}\right)\frac{1}{3} \le 1$ $k_\varepsilon = \frac{1}{1 + 110\varepsilon_1} \le 1$ $\varepsilon_1 = \varepsilon_x + (\varepsilon_x + 0.001)cot^2\beta$

The proportion of l_b supporting Strut *III* is given by:

$$\lambda_{III} = \frac{T_{s1}}{P+V} = \frac{a_{v1} + l_t}{0.9d \cdot cot\theta \cdot (1 + 1/\kappa)} = 1 - (\lambda_I + \lambda_{II}) \tag{8}$$

The tensile force T in the bottom longitudinal reinforcement at the support is given by:

$$T_{sup} = T_I + T_{II} + T_{III} \tag{9}$$

where T_I, T_{II} and T_{III} are respectively the horizontal components of force in Strut *I*, Strut *II* and Strut *III*.

$$T_I = P \cdot cot\beta_I \tag{10}$$

where β_I is the angle of Strut *I* (see Eq. (14)).

$$T_{II} = T_{s2} \cdot cot\beta_{II} = \frac{A_{sw}}{s_w} \cdot [0.9d \cdot cot\theta - (a_{v1} + l_t)] \cdot f_{yw} \cdot cot\beta_{II} \tag{11}$$

where β_{II} is the angle of Strut *II* (see Eq. (15)).

$$T_{III} = T_{s1} \cdot \cot\phi = \frac{A_{sw}}{s_w} \cdot (0.9d \cdot \cot\theta - a_{v2}) \cdot f_{yw} \cdot \cot\phi \tag{12}$$

where T_{s1} is the resultant tensile force in the stirrups within the inner shear span and ϕ is the angle of Strut *III* (see Eq. (16)).

The relative heights of the bottom node supporting Strut I and Strut II are given by:

$$\alpha_i = \frac{T_i}{T_{sup}} \tag{13}$$

where $i = I$ or *II*.

The angles of Strut *I* (β_I), Strut *II* (β_{II}) and Strut *III* (ϕ) can be calculated from geometry as follows:

$$cot\beta_I = \frac{\lambda_I \cdot 0.5l_b + \lambda_{II} \cdot l_b + a_{v1} + 0.5l_t}{h - c \cdot (\alpha_I + 2 \cdot \alpha_{II}) - \frac{T_{III} + 0.5T_I}{b \cdot f_{cnt}}} \tag{14}$$

$$cot\beta_{II} = \frac{\lambda_{II} \cdot 0.5l_b + e_{s2}}{h - c \cdot \alpha_{II} - \frac{T_I + T_{III} + 0.5T_{II}}{b \cdot f_{cnt}}} = \frac{\lambda_{II} \cdot 0.5l_b + a_{v1} + l_t + 0.5a_{v2}}{h - c \cdot \alpha_{II} - \frac{T_I + T_{III} + 0.5T_{II}}{b \cdot f_{cnt}}} \tag{15}$$

$$\cot\phi = \frac{(1 + \lambda_I + \lambda_{II}) \cdot 0.5l_b + e_{s1}}{h - c \cdot (1 + \alpha_I + \alpha_{II}) - \frac{0.5T_{III}}{b \cdot f_{cnt}}} = \frac{0.5 \cdot [(1 + \lambda_I + \lambda_{II}) \cdot l_b + a_{v1}]}{h - c \cdot (1 + \alpha_I + \alpha_{II}) - \frac{0.5T_{III}}{b \cdot f_{cnt}}} \tag{16}$$

where h is the beam height, c is the concrete cover measured from the bottom face of the beam to the centroid of the bottom longitudinal reinforcement, e_{s1} defines the position of the centroid of T_{s1} and e_{s2} defines the position of the centroid of T_{s2}. For the tested beams, $cot\theta$ is governed by failure of Strut *II* at its bottom end as follows:

$$cot\theta = \frac{1}{0.9d}\left[\frac{s_w}{A_{sw} \cdot f_{yw}} b \cdot f_{csb} \cdot (\alpha_{II} \cdot 2c \cdot cos\beta_{II} + \lambda_{II} \cdot l_b \cdot sin\beta_{II}) \cdot sin\beta_{II} + a_{v1} + l_t\right] \le cot\theta_{min} \tag{17}$$

If $cot\theta$ from Eq. (17) is greater than $cot\theta_{min}$ the maximum shear resistance is given by:

$$V_{max} = \frac{A_{sw} \cdot f_{yw}}{s_w} 0.9d.cot\theta_{min}(1 + 1/\kappa) \tag{18}$$

The equations of the STM can be readily solved with a nonlinear equation solver like the Generalised Reduced Gradient (GRG2) available in Microsoft Excel. The procedure for using GRG2 is to firstly estimate values for $cot\theta$, $cot\beta_I$, $cot\beta_{II}$ and $cot\phi$ which should be defined as variable cells. Updated values of the cotangents are then calculated with Eqs. (14) to (17) respectively using inputs from Eqs. (2) and (5)–(13) which can be directly evaluated. For example, once cotθ is known P is calculated in terms of V (see Eq. (2)) using Eq. (4). The solver GRG2 can then be used to adjust the trial values of $cot\theta$, $cot\beta_I$, $cot\beta_{II}$ and $cot\phi$ until the estimated values equal those given by Eqs. (14) to (17). Flexural failure also needs to be checked.

4.2. Derivation of design equations and solution for STMb

The maximum shear force transferred to the support by STMb is given by:

$$V_{Rd} = \lambda_t \cdot P + T_s = \lambda_t \cdot P + \frac{A_{sw}}{s_w} \cdot f_{yw} \cdot a_v = \frac{T_s}{1 - \lambda_b} = \frac{1}{(1 - \lambda_b)} \cdot \frac{A_{sw}}{s_w} \cdot f_{yw} \cdot a_v \tag{19}$$

where λ_t is the proportion of the top plate supporting the shear force carried by the direct strut, P is the applied point load, T_s is the tensile force in the stirrups within the inner shear span, A_{sw} is the cross sectional area of each set of stirrups at spacing s_w, f_{yw} is the yield strength of the stirrups, a_v is the clear shear span and λ_b is the relative length of the bottom plate supporting the shear force carried by the direct strut.

$$T_s = \frac{A_{sw}}{s_w} \cdot f_{yw} \cdot a_v = (1 - \lambda_t) \cdot P + V \tag{20}$$

where V is the uniform shear force. STMa applies if Eq. (20) is not satisfied.

Failure is assumed to occur due to simultaneous yielding of stirrups and crushing of strut *I* (direct strut) at the bottom node. Therefore, the applied load P is given by:

$$P = \frac{b \cdot f_{csb} \cdot (\alpha \cdot 2c \cdot cos\beta + \lambda_b \cdot l_b \cdot sin\beta) \cdot sin\beta}{\lambda_t} \tag{21}$$

where b is the beam width, f_{csb} is the concrete strength of Strut *I* at the bottom node, c is the concrete cover measured from the bottom face of the beam to the centroid of the bottom longitudinal reinforcement, l_b is the length of the bottom bearing plate, α is the relative proportion of the height of the bottom node supporting the horizontal component of Strut *I* and β is the angle of Strut *I*.

The ratio of the proportions of the bottom and top plate supporting the direct strut is given by:

$$\frac{\lambda_b}{\lambda_t} = \frac{1}{1 + \kappa} = \frac{P \cdot (1 - \lambda_b)}{T_s} \tag{22}$$

where κ is given by Eq. (2).

The force T in the longitudinal reinforcement at the outer edge of the loading plate is given by:

$$T = T_{sup} + Vcot\theta + (1 - \lambda_t) \cdot P \cdot cot\varphi \tag{23}$$

where θ is the orientation of the uniform compressive stress field, φ is the orientation of Strut *II* and T_{sup} is the tensile force in the longitudinal reinforcement at the support.

$$T_{sup} = T_I + T_{III} \tag{24}$$

where T_I and T_{III} are the horizontal components of force in Struts *I* and *III*.

$$T_I = \lambda_t \cdot P \cdot \cot\beta = \frac{\lambda_b}{1-\lambda_b} \cdot T_s \cdot \cot\beta = \frac{\alpha}{1-\alpha} \cdot T_s \cdot \cot\phi \quad (25)$$

where β is the orientation of Strut I and α defines the relative height of the bottom node supporting the horizontal component of the direct strut.

$$T_{III} = T_s \cdot \cot\phi \quad (26)$$

where ϕ is the orientation of Strut III and α is given by Eq. (13) with $i = I$.

$$cot\beta = \frac{\lambda_b \cdot 0.5 l_b + a_v + \lambda_t \cdot 0.5 l_t}{h - c \cdot \alpha - \frac{T_{III} + 0.5 T_I}{b \cdot f_{cnt}}} \quad (27)$$

$$\cot\phi = \frac{0.5 \cdot [(1+\lambda_b) \cdot l_b + a_v]}{h - c \cdot (1+\alpha) - \frac{0.5 T_{III}}{b \cdot f_{cnt}}} \quad (28)$$

where h is the beam height, a_v is the clear shear span, l_t is the top loading plate width and f_{cnt} is the flexural compressive stress.

In the tested beams, failure of STMb is governed by crushing of strut I at its bottom end. In this case, the coefficient α can be obtained by equating the horizontal component of force in strut I at failure to T_I from Eq. (25). This leads to:

$$\alpha = \frac{\lambda_b . l_b}{2c . cot\beta} \cdot \left[\frac{T_s (1 + cot^2\beta)}{(1-\lambda_b) . l_b . b . f_{csb}} - 1 \right] \quad (29)$$

STMb can be solved similarly to STMa with a nonlinear equation solver such as the Generalised Reduced Gradient (GRG2) solver in Microsoft Excel. The solution can also be found using the iterative procedure of Sagaseta and Vollum [2].

4.3. Shear resistance predictions of strut and tie models

The shear resistances of the tested beams were evaluated with STMa and STMb as appropriate. In STMa, the strength of strut *II* at its bottom end was initially related to the strut orientation β_{II} but slightly better failure load predictions were obtained when the strength was related to β_1. Justification for this is provided by [9,24,27] and Fig. 8.26b of prEN1992-1:21 [18] which relates the strut strength in a variable width stress field (e.g. fan) to the mean strut orientation with respect to the tie. Taking the strength of strut *II* as equal to that of strut *I* at the bottom node ensures that strut *I* is almost at failure when strut *II* fails, thereby allowing for redistribution of stress at the bottom node. For consistency with prEN1992-1:21 [18], the angle used to calculate the strength of strut *II* at its bottom node should be the least of β_1 and:

$$cot\theta_{cs} = \frac{cot\theta}{2} + \frac{l_b}{2 \cdot z} \quad (30)$$

The strength of beam 2P-1.1d/1.9d-50:50-4ϕ25s2 with two-point loads applied within 2d of a support was evaluated with the STM of Vollum and Fang [3]. Table 9 gives the resulting shear resistances calculated using the design concrete strengths given in Tables 6 to 8. In the cases of prEN1992-1:21 [18] and MCFT [23], the strut strength at the bottom node was calculated in terms of i) ε_x and ii) $0.5\varepsilon_x$ where ε_x is the peak strain in the flexural reinforcement at the bottom node. The latter approach is adopted in prEN1992-1:21 [18]. Table 9 shows that all the STM predictions are safe with the prEN1992-1:21 [18] predictions based on $0.5\varepsilon_x$ most accurate. The STMs predict greater strengths for comparable beams in the 2x3ϕ25s3 series than the 4ϕ25s2 series. This is principally due to the flexural reinforcement being provided in two layers in the 2x3ϕ25s3 series, which increases the bottom node depth. The reduction in ε_x due to the increase in flexural reinforcement area only accounts for around 10% of the strength increase. The increase in strut strength in the 2x3ϕ25s3 series due to the reinforcement being provided in two layers more than compensates for the increase in stirrup spacing compared with the 4ϕ25s2 series.

5. Modelling of beams with NLFEA

For comparison with the STM, the beams were modelled with NLFEA using 3D solid elements in ATENA [25]. The aim was to develop a calibrated modelling procedure that could be used to investigate other loading arrangements than tested. Concrete was modelled using CC3DNonLinCementitious2 [25] which is a fracture-plastic model that combines constitutive models for concrete in tension and compression. The optimum choice of concrete model parameters in CC3DNonLinCementitious2 is case-dependent and varies dependent on the tests selected for model calibration. Based on calibration studies by Pastore [20], a fixed crack model was adopted since this replicated the observed crack patterns best. Compressive fracture of concrete in CC3DNonLinCementitious2 is related to a critical compressive displacement, w_d, which was taken as its default value of 0.5 mm in ATENA [25] based on calibration studies by Pastore [20]. The concrete compressive strength is reduced in CC3DNonLinCementitious2 parallel to the crack direction, as in the MCFT [23]. The strength reduction is related to the largest maximal fracturing strain [25] and is limited to a ratio r_c of the uniaxial concrete compressive strength which was taken as 0.8. The reinforcing bars were modelled as discrete reinforcement using truss elements embedded in the solid concrete elements. Perfect bond was adopted between the reinforcement and concrete. The nodal displacements of the bar element are kinematically dependent on those of the solid element. A multi-linear stress–strain relationship was used to replicate the measured reinforcement stress strain relationship. Concrete and steel loading plates were meshed using eight node linear order hexahedra elements. The whole beam was modelled in the analyses using the same element size for concrete throughout the beam. A finite element size of

Table 9
Strut-and-tie predictions for short-span beams.

				V_{test}/V_{pred}				
				–	$0.5\varepsilon_x = T/(2E_sA_s)$		$\varepsilon_x = T/(E_sA_s)$	
beams	f_c (MPa)	V_{test} (kN)	ATENA [25] (FE)	EC2 [15] STM	MCFT [23]	prN1992:21 [18]	MCFT [23]	prEN1992:21 [18]
P-1.5d-4ϕ25s2[c]	28.5	387	0.83	1.19	1.12	0.95	1.21	1.03
2P-1.1d/1.9d-50:50-4ϕ25s2[d]	28.9	633	1.04	1.73	1.45	1.29	1.57	1.40
2P-1.5d/3d-40:60-4ϕ25s2[b]	29.0	492	1.05	1.51	1.46	1.26	1.56	1.36
2P-1.5d/3d-60:40-4ϕ25s2[b]	31.1	531	1.13	1.56	1.49	1.29	1.60	1.40
P-1.5d-2x3ϕ25s3[c]	30.8	496	1.01	1.25	1.25	1.01	1.35	1.11
2P-1.5d/3d-40:60-2x3ϕ25s3[a]	31.0	510	1.11	1.33	1.37	1.16	1.47	1.25
2P-1.5d/3d-20:80-2x3ϕ25s3[a]	31.1	387	1.03	1.16	1.22	1.08	1.28	1.12
		Mean	1.03	1.39	1.33	1.15	1.43	1.24
		StdDev	0.10	0.22	0.14	0.14	0.16	0.15
		CoV	9%	16%	11%	12%	11%	12%

[a] : STMa, [b]: STMb, [c]: STM of Sagaseta and Vollum [2], [d]: STM of Vollum and Fang[3].

50 mm^3, giving 10 elements through the beam depth, was chosen on the basis of a sensitivity study that considered cubic element sizes of 25 mm^3, 50 mm^3 and 75 mm^3. The point loads were applied through the central node on the top surface of the loading plate. Vertical constraints were applied to the centre line of the bottom surface of bearing plates, allowing the supports to rotate about this line. Horizontal movements were constrained in the longitudinal direction at one bearing plate and in the transverse direction at the other bearing plate. All plates were modelled as elastic with modulus of 200 GPa. Load was applied in force control using the arc-length solution procedure. The adopted modelling parameters were determined by best fitting the NLFEA results to a series of similar, but short shear span, beams with shear reinforcement tested by Vollum and Fang [3]. Full details of the calibration study are given by Pastore [20]. Table 10 summarises the key user defined parameters adopted in modelling the tested beams. Other parameters in CC3DNonLinCementitious2 were taken as the default values from [25] given in Table 11. The calibrated NLFEA model was used to determine the predicted strengths of the eight beams tested in this campaign. The resulting failure loads are seen to compare reasonably well with the measured ones as shown in Table 9. Fig. 10 compares the measured and predicted load displacement responses of the calibrated model for test series 2 at LVDT 6 positioned under P_2 at $3d$. Overall, the comparison is favourable even though the initial NLFEA response is overly stiff. Further details of the NLFEA verification including comparison of measured and predicted reinforcement strains is given by Pastore [20].

6. Evaluation of shear enhancement methods in MC2010 [17] and prEN1992-1:2021 [18]

As well as allowing design by STM, design standards give simplified formulae for modelling shear enhancement near supports of top loaded beams. This section considers the simplified design methods of MC2010 [17] Level of Approximation III (LoA III) (see Appendix A) and pr EN1992-1:2021 [18]. EC2 [15] is not considered since it is known to perform poorly for beams with shear reinforcement [2,3].

The draft next generation EC2 (prEN1992-1:2021 [18]) calculates the shear resistance of beams with shear reinforcement (τ_{Rd}) as follows:

$$\tau_{Rd} = \frac{V_{Rd}}{b_w z} = \frac{A_{sw}}{b_w s} f_{ywd} cot\theta = \rho_w f_{ywd} cot\theta \le \frac{\nu \eta_{fc} f_{cd}}{2} \tag{31}$$

where V_{Rd} is the design shear resistance, b_w is the width of the web, $z = 0.9d$ is the lever arm for shear calculation, $f_{cd} = f_{ck}/\gamma_c$ where γ_c is the partial factor for concrete which is taken as 1.0 in this paper, η_{fc} is defined in Table 8, f_{ywd} is the design yield strength of the shear reinforcement and:

$$cot\theta_{min} \ge cot\theta = \sqrt{\frac{\nu \eta_{fc} f_{cd}}{\rho_w f_{ywd}} - 1} \ge 1 \tag{32}$$

For beams without axial force, ν may be taken as 0.5 with $cot\theta_{min} = 2.5$. Alternatively [18], $cot\theta$ can be taken as greater than $cot\theta_{min} = 2.5$, or

Table 10
Summary of best fitted parameters for numerical modelling of tested beams.

Parameter	Beams with stirrups ATENA v5.6.1i
Smeared crack model	Fixed crack model (1.0)
Shear factor	3000
Compressive strength of concrete	Cylinder strength ($f_{cm} \cong$ 30 MPa)
Tensile strength of concrete	Brazilian test ($f_{ctm} \cong$ 2.2 MPa)
Maximum aggregate size	20 mm
Critical plastic displacement w_d	0.5 mm
Compressive strength reduction factor r_c	0.8
Mesh size	50 mm
Element	8-node brick
Load step size (initial increment)	1% P_u (experimental failure load)
Solution method	Arc-length

Table 11
Default values of main model parameters.

Parameter	Formula or value
Modulus of elasticity (MC 2010)	$E_{ci} = 21.5 \cdot 10^3 \cdot (f_{cm}/10)^{\frac{1}{3}}$ in MPa
Poisson's ratio	0.2
Fracture Energy (MC2010)	$G_F = 73 \cdot f_{cm}^{0.18}$ in N/m
Plastic strain	$\varepsilon_{cp} = f_{cm}/E_{ci}$
Onset of crushing	$f_{c0} = -2 \cdot f_{ctm}$ in MPa
Direction of the plastic flow	$\beta = 0$
Roundness of failure surface	$EXC = 0.52$

$\nu > 0.5$ if the effectiveness factor is calculated as:

$$\nu = \frac{1}{1 + 110[\varepsilon_x + (\varepsilon_x + 0.001) cot^2\theta]} \le 1 \tag{33}$$

where ε_x is the average of the strain in the bottom and top chords accounting for sign. The forces in the tension and compression chords are given respectively by $F_{td} = M/z + 0.5N_{vd} \le M_{max}/z$ and $F_{cd} = M/z - 0.5N_{vd}$ where z is the flexural lever arm, which for calculation of ε_x is approximated as $0.9d$ in this paper, and $N_{vd} = V cot\theta$. Strains in the tension and compression chords are calculated as $F_{td}/(A_s E_s)$ and $F_{cd}/(A_c E_c)$ respectively where A_c is the area of the compressive chord which is calculated for a fully cracked section in this paper assuming elastic behaviour.

For beams with stirrups, prEN1992-1:2021 [18] utilises a stress field approach [26] to calculate the enhanced shear strength of beams loaded with concentrated loads applied within $z cot\theta$ of supports. The enhanced shear resistance is assumed to equal the sum of a direct strut contribution plus the force carried by the vertical steel links over the clear shear span a_v. For cotθ ≥ 1, the shear resistance is given [18] by:

$$V_{Rd} = b_w z \nu \eta_{fc} f_{cd} \frac{cot\theta - cot\beta}{1 + cot^2\theta} + \frac{A_{sw}}{s} z f_{ywd} cot\beta \le b_w z \nu \eta_{fc} f_{cd} \frac{cot\theta}{1 + cot^2\theta} \tag{34}$$

where b_w is the beam web width, z is the internal lever arm taken as 0.9 times the effective depth, ν is a strength reduction factor, θ is the orientation of the compression field, $cot\beta = a_v/z$ where a_v is the clear shear span, A_{sw} is the cross-sectional area of each set of stirrups at spacing s and f_{ywd} is the design yield strength of the stirrups. For $1 \le$ cotθ $\le cot\theta_{min} = 2.5$, the effectiveness factor ν may be taken as 0.5. In this case, the optimum value of cotθ in Eq. (34) is given [18] by:

$$cot\theta = cot\beta + \sqrt{1 + cot^2\beta} \le cot\theta_{min} \tag{35}$$

Alternatively, the effectiveness factor ν in Eq. (34) may be calculated using Eq. (33) in terms of the strain ε_x at a cross section midway between the support and load. In this case, the bending moment used in the calculation of the tension (F_{td}) and compression (F_{cd}) chord forces should be taken as $M+\Delta M$ where M is the design bending moment at the considered cross section and ΔM is given by:

$$\Delta M = \left(V_{Ed} - \frac{A_{sw}}{s} z f_{ywd} cot\theta \right) a \tag{36}$$

where a is the distance from the centreline of the support to the centreline of the concentrated load under consideration.

For the tested beams with two-point loads, shear failure needs to be checked for the shear force i) between the support and P_1 and ii) between P_1 and P_2 (see Fig. 2). For beams loaded at $1.5d$ and $3d$, the shear resistance between P_1 and P_2 is the unenhanced shear resistance. The shear resistance predictions are shown in Table 12 for MC2010 [17] LoAIII and prEN1992:2021 [18] with $\nu = 0.5$ and with ν from Eq. (33). Also shown for comparison are the predictions from ATENA and STM prEN1992:21 with $0.5\varepsilon_x$. The resistances were all calculated with partial factors equal to 1.0 for concrete and reinforcement. Table 12 shows that the shear enhancement methods of MC2010 [17] and prEN1992 [18]

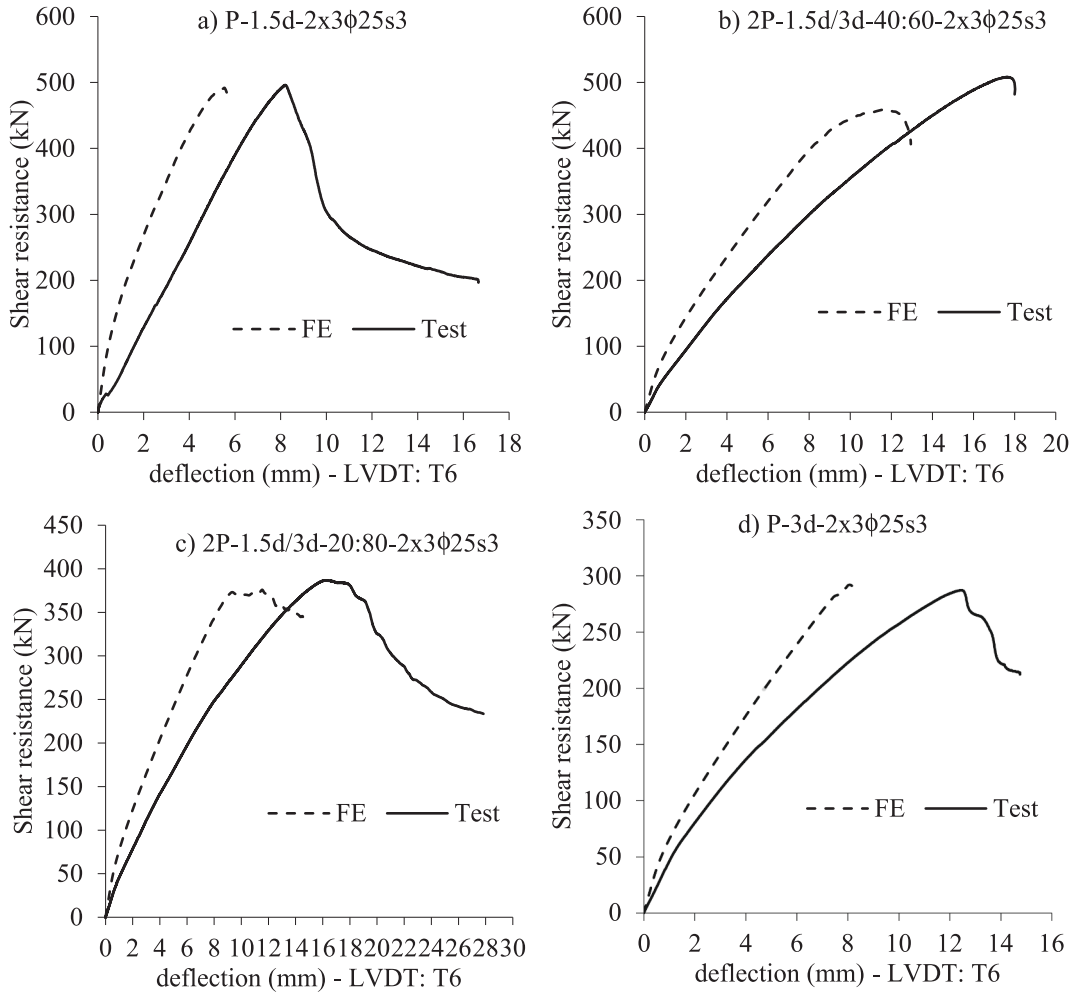

Fig. 10. Comparison of measured and predicted load deflection curves for series 2.

Table 12
Design code predictions for all beams.

beams with stirrups	f_c (MPa)	V_{test} (kN)	$V_{test\ max}/V_{pred\ max}$ ATENA [25]	prEN1992:21 $0.5\varepsilon_x$ STM	MC2010 LoA III [17]	prEN1992:21 $\nu = 0.5$ [18]	prEN1992:21 calculate ν [18]
P-1.5d-4ϕ25s2	28.5	387	0.83	0.95	1.00	1.05	1.10
2P-1.1d/1.9d-50:50-4ϕ25s2	28.9	633	1.04	1.29	1.61	1.50	1.38
2P-1.5d/3d-40:60-4ϕ25s2	29.0	492	1.05	1.26	1.57	1.31	1.45
P-3d-4ϕ25s2	29.0	297	0.93	–	1.21	1.13	0.99
2P-1.5d/3d-60:40-4ϕ25s2	31.1	531	1.13	1.29	1.49	1.36	1.47
P-1.5d-2x3ϕ25s3	30.8	496	1.01	1.01	1.58	1.60	1.59
P-3d-2x3ϕ25s3	30.9	287	0.98	–	1.35	1.74	1.23
2P-1.5d/3d-40:60-2x3ϕ25s3	31.0	510	1.11	1.16	1.93	1.63	1.70
2P-1.5d/3d-20:80-2x3ϕ25s3	31.1	387	1.03	1.08	1.58	1.61	1.31
		Mean	1.01	1.15	1.48	1.44	1.36
		StdDev	0.09	0.14	0.27	0.24	0.23
		CoV	9%	12%	18%	17%	17%

are of comparable accuracy despite the differences in their formulation. Calculating ν with Eq. (33) allows significantly lower strut inclinations θ_{min} for beams P-3d-4ϕ25s2 and P-3d-2x3ϕ25s3 which increases their shear resistance significantly over taking $\cot\theta_{min} = 2.5$. However, calculating ν gives lower resistances for the other beams since ν from Eq. (33) is less than 0.5.

7. Discussion

Eq. (34) of prEN1992-1:2021 [18] is derived from consideration of the free body diagram shown in Fig. 11 [26]. The shear resistance at the support is given by the sum of the vertical component of the force in the direct strut, which is assumed to have inclination θ and the force in the

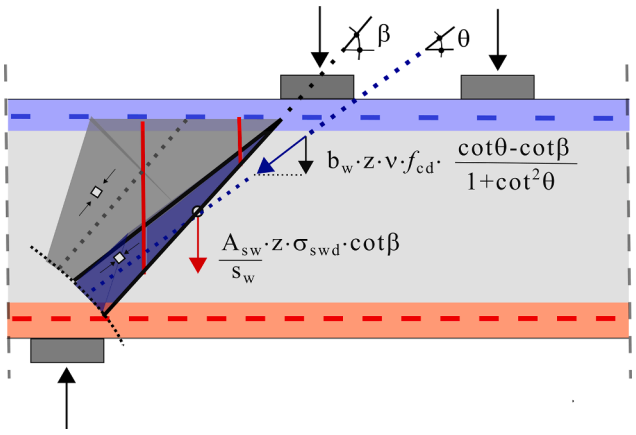

Fig. 11. Stress field used in derivation of equation (34) [26].

stirrups within the clear shear span a_v. This approach has some similarity to that of the superseded UK code BS8110 [16] which relates shear resistance to the angle of the critical failure plane. Both these methods imply that the shear resistance along the considered failure plane is independent of the ratio between the loads P_1 and P_2 in Fig. 2. This assumption is inconsistent with the STM in Fig. 8 as well as the shear enhancement method of MC2010 [17]. In both these approaches, shear enhancement only applies to the proportion of P_1 that contributes to the design shear force in the shear span under consideration. Conversely, the enhanced shear resistance given by the draft EN1992 [18] is independent of the proportion of the shear force at P_1 that arises from P_2 in Fig. 2. A further difference between the simplified shear enhancement methods and STM is that the shear resistance of the STM depends on the size of the bearing plates and the cover to the centroid of the flexural reinforcement.

The influence of the loading ratio $P_1/(P_1 + P_2)$ on shear resistance was explored further by carrying out a parametric study on beams with the same cross section and span as tested. The load P_1 was placed at 1.5d from the centreline of the left hand support while P_2 was placed at 3d from the left hand support as in the tests. The ratio $P_1/(P_1 + P_2)$ was varied from 0 to 100% in steps of 10%. The flexural reinforcement was taken as either 4B25 (4ϕ25) bars or 6B25 (2x3ϕ2) bars in two layers of three as in the tests. 8 mm stirrups were used as in the tests with spacing of 100 mm (2P-1.5d/3d-2x3ϕ25s100), 200 mm (2P-1.5d/3d-4ϕ25s200) and 300 mm (2P-1.5d/3d-2x3ϕ25s300). The concrete cylinder compressive strength was taken as 30 MPa since this is close to the average concrete compressive strength in the tests. Reinforcement strengths were as in the tests.

The beams were analysed with NLFEA, STM (prEN1992-1:21 [18]: $0.5\varepsilon_x = T/(2E_sA_s)$) as well as the shear enhancement methods of MC2010 [17] LoA III and prEN1992-1:21 [18] using mean material strengths. The maximum shear forces at failure are plotted against the percentage of the total load applied at P_1 (see Fig. 2) in Fig. 12 a) to c) which also show measured beam strengths and the shear force at flexural failure. The flexural limit was not applied to the code predictions when calculating V_{max} in order to better illustrate the predicted influence of loading arrangement on shear resistance. Hence, the shear capacity in Fig. 12 is given by the least of the plotted shear forces at shear and flexural failure. The NLFEA strengths agree very well with the measured strengths with the next best predictions obtained with the STM. The STM strengths are relatively high in Fig. 12c for beam 2P-1.5d/3d-2x3ϕ25s3 due to the flexural reinforcement being provided in two layers. This increases the strut width at the bottom node as previously discussed in the context of the proportionally greater STM strengths predicted for the tested 2x3ϕ25s3 series compared with the tested 4ϕ25s2 series. Generally, the NLFEA and STM strength predictions are reasonably independent of loading ratio for $P_1/(P_1 + P_2)$ between 50% and 100%.

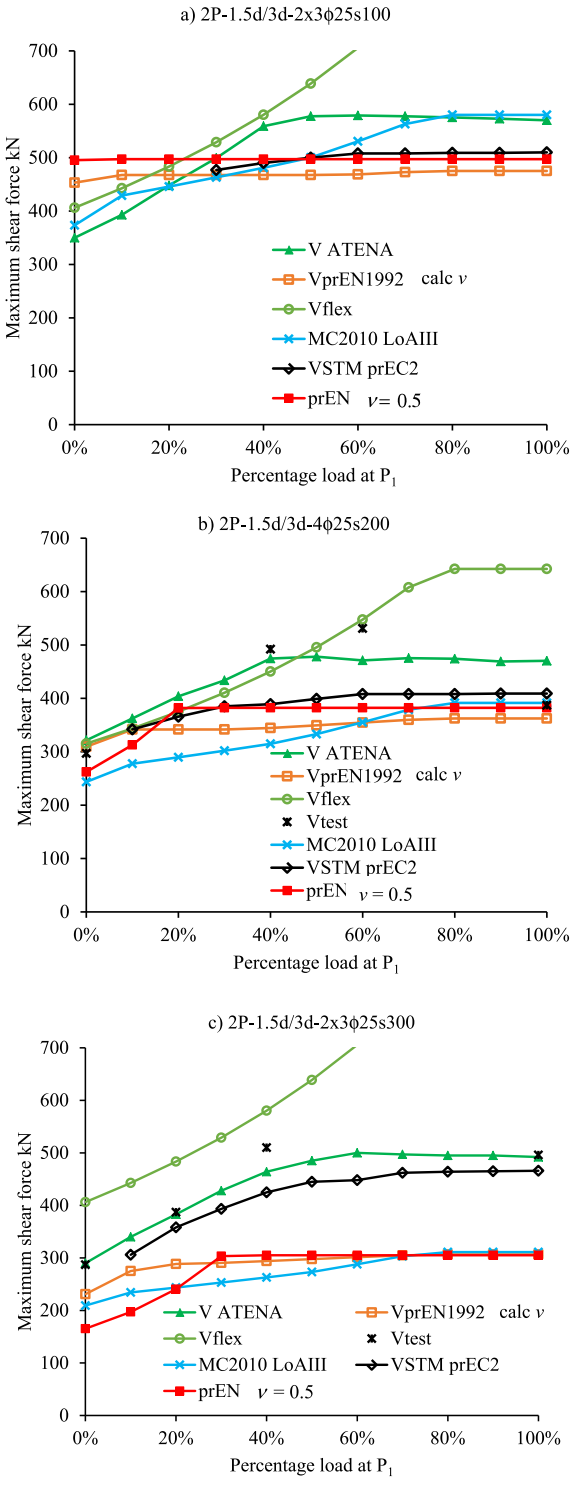

Fig. 12. Influence of loading ratio on shear resistance for a) 2P-1.5d/3d-2x3ϕ25s100, b) 2P-1.5d/3d-4ϕ25s200 and c) 2P-1.5d/3d-2x3ϕ25s300.

Below this ratio the shear resistance reduces. According to the STM this is because the proportion of load being transferred to the support by the direct strut progressively reduces as the load ratio $P_1/(P_1 + P_2)$ reduces. The strength enhancement factor of MC2010 [17] reduces similarly with load ratio because it only applies to P_1 and not the shear force coming from P_2.

The maximum shear resistance in Fig. 12 predicted by prEN1992-1:21 [18] with $\nu = 0.5$ only reduces when shear failure becomes critical between P_1 and P_2 owing to Eq. (31) governing. This is due to the

shear resistance given by Eq. (34), which applies between the support and P_1, being independent of the proportion of maximum shear force arising from P_1. Calculating ν in terms of the reinforcement strain in Eq. (34) of prEN1992-1:2 1[18] gives slightly lower values of V_{max} for the considered beams than the standard method with $\nu = 0.5$ when the critical section lies between the support and P_1. This is because the calculated value of ν is less than 0.5 for these beams unlike beam 2P-1.1d/1.9d-50:50-4ϕ25s2 (see Table 12) where the failure plane is steeper. The key benefits of calculating ν arise in Fig. 12 for $P_1/(P_1 + P_2)$ less than 20% where calculating ν allows $cot\theta_{min}$ to be increased above 2.5. Despite not capturing the experimentally observed drop in V_{max} with reducing $P_1/(P_1 + P_2)$, prEN1992-1:21 [18] tends to give slightly better predictions of the maximum shear force at failure (which is limited by flexure) than MC2010 [17] LoAIII. The prEN1992:21 [18] method scores highly for ease of use when $\nu = 0.5$ compared with MC2010 [17] since it is simpler to enhance the shear resistance than reduce the design shear force resulting from arching action. This is especially true for moving concentrated loads. A potential disadvantage of the prEN1992-1:21 [18] method is that unlike MC2010 [17] it doesn't differentiate between top and bottom loading within $zcot\theta$ of the support. In Fig. 11, only top loading would be resisted by the direct strut which gives rise to shear enhancement.

8. Conclusions

This paper investigates the influence of loading arrangement on shear enhancement in simply supported reinforced concrete beams with shear reinforcement. The main focus is on load arrangements comprising concomitant point loads applied simultaneously at 1.5d and at 3d from the support with greatest shear force. This type of loading arrangement in which shear enhancement only applies to part of the load is common in practice but to the authors' knowledge has not previously been systematically investigated. Experimental results for nine tests on eight beams are presented and compared with the strength predictions of NLFEA with ATENA [25], STM, MC2010 LoAIII [17] and prEN1992-1:21 [18]. The key findings are as follows:

- Shear resistance increases as the failure plane becomes steeper as illustrated by comparison of the shear strengths of beams P-1.5d-4ϕ25s2 (387 kN) and 2P-1.1d/1.9d-50:50-4ϕ25s2 (633 kN) with statically equivalent loading. The horizontal projection of the failure plane was 562.5 mm for beam P-1.5d-4ϕ25s2 but only 375 mm for 2P-1.1d/1.9d-50:50-4ϕ25s2. This observation is consistent with the design approach of prEN1992-1:21 [18] for shear enhancement in beams with shear reinforcement.
- The most accurate strength predictions of the tested beams were obtained with NLFEA and STM with strut strengths calculated with prEN1992-1:21 [18] in terms of $0.5\varepsilon_x$ where ε_x is the flexural reinforcement strain at the inside edge of the support.
- The measured shear resistance of the beams loaded simultaneously with point loads P_1 at 1.5d and P_2 at 3d is relatively constant for $P_1/(P_1 + P_2) \geq 40\%$ and can be conservatively assumed to equal that for $P_1/(P_1 + P_2) = 100\%$ which simplifies the development of STM. For lower loading ratios, the shear resistance reduces almost linearly to that corresponding to 100% of the load at 3d.
- The length of the plateau over which shear resistance is relatively constant is overestimated by prEN1992-1:21 [18] since it neglects the interaction between P_1 and P_2 which causes shear resistance to reduce prior to becoming critical, according to [18], between P_1 and P_2. Despite this, the shear enhancement provisions of prEN1992-1:21 [18] were found to be sufficiently accurate for practical purposes and easier to apply than the shear enhancement rules of MC2010 LoAIII [17].
- Due to the limited nature of the experimental campaign further tests are suggested for detailed study of the influence of parameters such as relative dimensions of beam and support plates, shear span, shear reinforcement ratio and concrete strength.

CRediT authorship contribution statement

Marcus Vinicius Filiagi Pastore: Investigation, Data curation, Formal analysis, Validation, Visualization, Writing – original draft, Writing – review & editing. **Robert Lars Vollum:** Conceptualization, Methodology, Supervision, Project administration, Resources, Funding acquisition, Writing – review & editing.

Declaration of Competing Interest

The authors declare that they have no known competing financial interests or personal relationships that could have appeared to influence the work reported in this paper.

Acknowledgement

The first author wishes to acknowledge the financial support of the National Council for Scientific and Technological Development (CNPq), through the Science Without Borders Programme, funded by the Brazilian Ministry of Science and Technology.

Appendix A. Model code 2010 shear resistance

In MC2010 [17] LoAIII, the design shear resistance in the range of $V_{Rd} \leq V_{Rd,max}(\theta_{min})$ is given by:

$$V_{Rd} = V_{Rd,c} + V_{Rd,s} \tag{A1}$$

$$V_{Rd,c} = k_v \cdot \frac{\sqrt{f_{ck}}}{\gamma_c} \cdot z \cdot b_w \tag{A2}$$

in which $\sqrt{f_{ck}}$ should not be taken as greater than 8 MPa.

$$\theta_{min} = 20^{\circ} + 10000 \cdot \varepsilon_x \tag{A3}$$

$$k_v = \frac{0.4}{1 + 1500\varepsilon_x} \cdot \left[1 - \frac{V_{Ed}}{V_{Rd,max}(\theta_{min})}\right] \geq 0 \tag{A4}$$

$$\varepsilon_x = \frac{1}{2E_s A_{sl}} \cdot \left(\frac{M_{Ed}}{z} + V_{Ed}\right) \leq \frac{M_{max}}{2E_s A_{sl} z} \tag{A5}$$

where E_s is the Young's modulus of the longitudinal reinforcement, A_{sl} is the area of flexural tension reinforcement, z is the lever arm which may be taken as 0.9d for shear, M_{Ed} is the design bending moment taken at d from the support or concentrated load but not closer than d from the face of the support and M_{max} is the maximum beam moment. The upper limit on ε_x of $\varepsilon_x \leq \frac{M_{max}}{2E_s A_s z}$ is not given in MC2010 [17] but is implicit in its design model for shear.

$$V_{Rd,s} = \frac{A_{sw}}{s} z f_{yd} cot\theta \leq V_{Rd,max} \tag{A6}$$

$$V_{Rd,max} = k_c \frac{f_{ck}}{\gamma_c} b_w z sin\theta cos\theta \tag{A7}$$

$$k_c = k_\varepsilon \eta_{f_c} \tag{A8}$$

$$k_\varepsilon = \frac{1}{1.2 + 55\varepsilon_1} \leq 0.65 \tag{A9}$$

$$\eta_{f_c} = \left(\frac{30}{f_{ck}}\right)^{\frac{1}{3}} \leq 1 \tag{A10}$$

$$\varepsilon_1 = \varepsilon_x + (\varepsilon_x + 0.002) cot^2\theta \tag{A11}$$

If $V_{Rd} \geq V_{Rd,max}(\theta_{min})$ the design shear resistance is given by Eq. (A7).

MC2010 [17] models shear enhancement by reducing the shear force component of loads acting at a distance a_i from the centre of the support, with clear shear span $a_{vi} \leq 2d$ by the multiple:

$$\beta_i = \frac{a_{vi}}{2d} \geq 0.5 \tag{A12}$$

where a_{vi} is the clear shear span measured to concentrated load P_i and d is the beam effective depth.

References

[1] Todisco L, Reineck KH, Bayrak O. European design rules for point loads near supports evaluated with data from shear tests on non-slender beams with vertical stirrups. Struct Concr 2016;17(2):135–44.
[2] Sagaseta J, Vollum RL. Shear design of short-span beams. Mag Concr Res 2010;62 (4):267–82.
[3] Vollum RL, Fang L. Shear enhancement in RC beams with multiple point loads. Eng Struct 2014;80:389–405.
[4] Elwakeel A, Vollum R. Shear enhancement in RC cantilevers with multiple point loads. Mag Concr Res 2021;74(10):507–27. https://doi.org/10.1680/jmacr.19.00566.
[5] Chen H, Yi W-J, Hwang H-J. Cracking strut-and-tie model for shear strength evaluation of reinforced concrete deep beams. Eng Struct 2018;163:396–408.
[6] Brown MD, Bayrak O. Investigation of deep beams with various load, configurations. ACI Struct J 2007;104(5):611–20.
[7] Amini Najafian H, Vollum RL, Fang L. Comparative assessment of finite-element and strut and tie based design methods for deep beams. Mag Concr Res 2013;65 (16):970–86.
[8] Ismail KS, Guadagnini M, Pilakoutas K. Numerical investigation of the shear strength of RC deep beams using the microplane model. J Struct Eng 2016;142(10): 04016077.
[9] Mihaylov BI, Bentz EC, Collins MP. Two-parameter kinematic theory for shear behavior of deep beams. ACI Struct J 2013;110(3):447–55.
[10] Choi KK, Kim JC, Park HG. Shear strength model of concrete beams based on compression zone failure mechanism. ACI Struct J 2016;113(5):1095–106.
[11] Bairán JM, Menduiña R, Marí A, Cladera A. Shear strength of non-slender reinforced concrete beams. ACI Struct J 2020;117(2):277–89.
[12] Brown MD, Bayrak O, Jirsa JO. Design for shear based on loading conditions. ACI Struct J 2006;103(4):541–50.
[13] Ferguson PM. Some implications of recent diagonal tension tests. ACI J Proc 1956; 53(8):157–72.
[14] Bryant RH, Bianchini AC, Rodrguez JJ, Kesler KE. Shear strength of two-span continuous reinforced concretet beams with multiple point loading. ACI J Proc 1962;59(9):1143–78.
[15] BSI (British Standards Institution). BS EN 1992-1-1:2004: Eurocode 2: Design of concrete structures. Part 1-1, General rules and rules for buildings. London: BSI.
[16] BSI (British Standards Institution). BS 8110:1997: Structural use of concrete. Part 1. London: BSI.
[17] fib Model Code for Concrete Structures 2010, Ernst & Sohn; 2013.
[18] prEN 1992-1-1:2021-09 Eurocode 2: design of concrete structures—part 1–1: general rules, rules for buildings, bridges and civil engineering structures. Brussels: Comité Européen de Normalisation 2021.
[19] BSI (British Standards Institution). BS EN ISO 15630-1:2010 Steel for the reinforcement and prestressing of concrete - test methods. Reinforcing bars, wire rod and wire, London: BSI.
[20] Pastore MVF. Influence of loading arrangement on shear enhancement of reinforced concrete beams, thesis (PhD), Imperial College London; 2020.
[21] LaVision. 'DaVis 10.0 Software', Product Manual; 2019.
[22] Muttoni A. (The Applicability of the Theory of Plasticity in the Design of Reinforced Concrete (in German: "Die Anwendbarkeit der Plastizitätstheorie in der Bemessung von Stahlbeton"), thesis (PhD), ETH Zürich; 1989.
[23] Vecchio FJ, Collins MP. The modified compression-field theory for reinforced-concrete elements subjected to shear. J Am Concr Instit 1986;83(2):219–31.
[24] Fernandez Ruiz M, Muttoni A. Background document to subsection 8.5: Design with strut-and-tie models and stress fields. In: CEN/TC250/SC2/WG1/TG4 for prEN 1992-1-1:2020-11(D7), Report EPFL-IBETON 17-01-R2; 24 Feb 2021.
[25] Cervenka V, Cervenka J, Jendele L. ATENA Program Documentation, Part 1. Theory. Prague: Cervenka Consulting; 2020. p. 350.
[26] Muttoni A, Fernandez Ruiz M, Pejatovic M. Background document to subsection 8.2.3: Members requiring design shear reinforcement. In: CEN/TC250/SC2/WG1/TG4 for prEN 1992-1-1:2020-11(D7), Report EPFL-IBETON 17-01-R1; 26 Feb 2021.
[27] https://onlinepubs.trb.org/onlinepubs/nchrp/docs/NCHRP20-07(306)_FR.pdf; 2013. [Accessed 20 May 2022].